THE PLANETARY SCIENCE JOURNAL, 6:59 (19pp), 2025 March https://doi.org/10.3847/PSJ/adb4f4

A Pre-flyby View on the Origin of Asteroid Donaldjohanson, a Target of the NASA Lucy Mission

Simone Marchi[1], David Vokrouhlický[2], David Nesvorný[1], William F. Bottke[1], Josef Ďurech[2], and Harold F. Levison[1]

[1] Department of Space Studies, Southwest Research Institute, 1050 Walnut St., Suite 300, Boulder, CO 80302, USA; marchi@boulder.swri.edu
[2] Astronomical Institute, Charles University, V Holešovičkách 2, CZ 18000, Prague 8, Czech Republic
Received 2024 December 17; revised 2025 February 6; accepted 2025 February 10; published 2025 March 17

Abstract

The NASA Lucy mission is scheduled to fly by the main-belt asteroid (52246) Donaldjohanson on 2025 April 20. Donaldjohanson (DJ hereafter) is a member of the primitive (C-type class) Erigone collisional asteroid family located in the inner main belt in proximity of the source regions of asteroids (101955) Bennu and (162173) Ryugu, visited respectively by the OSIRIS-REx and Hayabusa2 missions. In this paper we provide an updated model for the Erigone family age and discuss DJ evolution resulting from nongravitational forces (namely Yarkovsky and Yarkovsky–O'Keefe–Radzievski–Paddack (YORP)), as well as its collisional evolution. We conclude that the best-fit family age is 155 Myr and that, on such timescales, both Yarkovsky and YORP effects may have affected the orbit and spin properties of DJ. Furthermore, we discuss how the NASA Lucy mission could provide independent insights on such processes, namely by constraining DJ shape, surface geology, and cratering history.

Unified Astronomy Thesaurus concepts: Main belt asteroids (2036)

1. Introduction

(52246) Donaldjohanson (hereafter DJ for short) is a primitive inner main-belt asteroid (spectrally C-type class), with an estimated average diameter ranging from 3 to 5 km (e.g., J. R. Masiero et al. 2011). DJ is thought to be a member of the Erigone collisional family, which has been estimated to have formed between about 130 and 270 Myr ago (e.g., D. Vokrouhlický et al. 2006b; W. F. Bottke et al. 2015b; F. Spoto et al. 2015; A. Milani et al. 2019). The Erigone family is located in the inner part of the main belt, close to several other collisional families of similar spectral taxonomy (Figure 1). These include the New Polana and Eulalia families, which are believed to be the respective source families for primitive asteroids (101955) Bennu and (162173) Ryugu, visited by the NASA OSIRIS-REx and JAXA Hayabusa2 space missions (see, e.g., W. F. Bottke et al. 2015b; E. Tatsumi et al. 2021; D. Takir et al. 2024). Unlike New Polana and Eulalia, both crossed by the powerful J3/1 mean motion resonance with Jupiter, the Erigone family is located in a less favorable position to deliver near-Earth objects and meteorites to Earth. This raises the intriguing scientific question as to whether DJ is structurally and compositionally similar to Bennu/Ryugu (and any known primitive meteorite group), or whether it has distinct properties.

Furthermore, DJ itself appears to be a peculiar object. Ground-based observations reveal a large light-curve amplitude of $\simeq 1$ mag and a rather long rotation period of $\simeq 252$ hr (e.g., M. Ferrais et al. 2021). A possible interpretation is that DJ is quite elongated (a/c body axis ratio ~ 3) and that it is a slow rotator, possibly due to thermal torques that have decelerated its spin rate over time (e.g., D. Vokrouhlický et al. 2007, and Section 2.2). Both of these characteristics are very distinct from Bennu and Ryugu ($a/c \simeq 1.1$ for both objects and periods of $\simeq 4.3$ and $\simeq 7.6$ hr, respectively; e.g., J. H. Roberts et al. 2021).

A possible explanation for these bulk differences has to do with a different formation mechanism. For instance, it has been suggested that the Erigone family was formed by a sizable cratering event (e.g., A. Milani et al. 2019), while both the New Polana and Eulalia families were produced by catastrophic disruption events (e.g., W. F. Bottke et al. 2015b). Depending on the circumstances, this difference might suggest that DJ is a more competent body (perhaps retaining some internal strength) rather than being a rubble pile such as Bennu and Ryugu. Another possibility is that DJ is a less collisionally evolved object based on its relatively young family age and larger size (less than ~ 270 Myr and ~ 4 km size), while the much older ages of the New Polana (~ 1400 Myr) and Eulalia (~ 850 Myr) families could have resulted in subsequent collisional evolution for Bennu and Ryugu (about 0.49 and 0.90 km in diameter, respectively). Finally, it is possible that there are compositional differences that could affect the formation and bulk properties of these objects. Regarding the latter, a recently published visible−near-IR (0.5−2.5 μm) spectra of DJ has shown possible distinctive characteristics compared to Bennu and Ryugu, but the poor signal-to-noise ratio does not allow for any definitive conclusions (see B. Harvison et al. 2024).

Some of these open issues can be tested by the NASA Lucy spacecraft, which will encounter DJ on 2025 April 20 at a close-approach distance of about 900 km and a relative velocity of 13.4 km s^{-1} (H. F. Levison et al. 2021). The flyby will provide a unique opportunity to image DJ at a highest resolution of about 10 m pixel^{-1}. The acquired imaging data will be utilized to study DJ's morphology and crater population. We anticipate that the quality of the data will be comparable to what was obtained by Lucy during the recent flyby of main-belt asteroid (152830) Dinkinesh (H. F. Levison et al. 2024). The anticipated cratering data will be used to constrain DJ's collisional history and possibly provide an

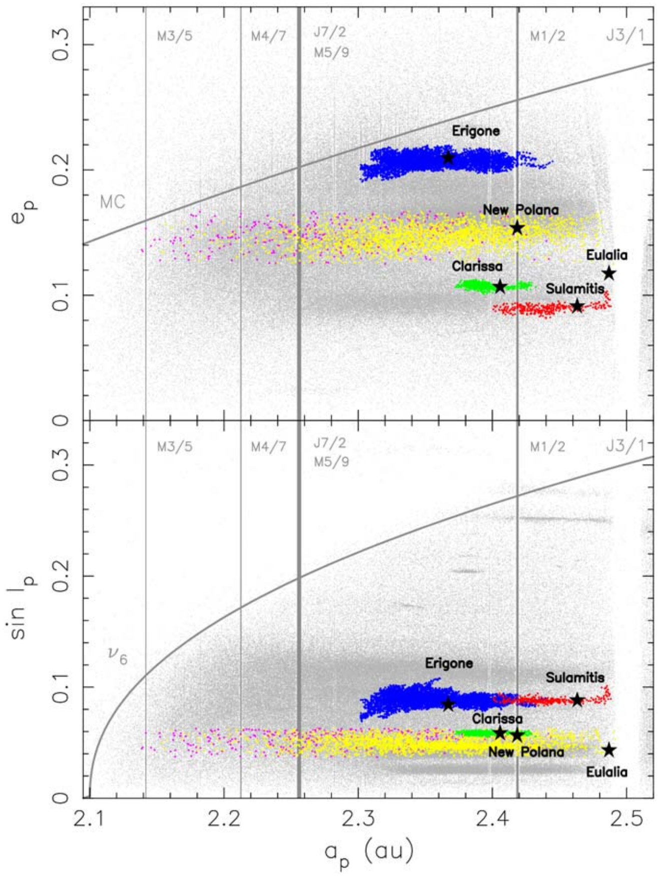

Figure 1. Population context of asteroid DJ, a member of the C-type Erigone family (blue). Intriguingly, several other C-type families are also located in this region of the main belt, including New Polana and Eulalia, the likely source of spacecraft-visited asteroids (101955) Bennu and (162173) Ryugu, respectively (see text). These families are highlighted (in violet and yellow, respectively), while the remaining population of asteroids (mostly S-types) is shown using the light-gray symbols. The abscissa is the proper semimajor axis a_P, and the ordinate is the proper eccentricity e_P (top panel) and proper sine of inclination $\sin I_P$ (bottom panel). Several orbital resonances are indicated (secular resonance ν_6, Jupiter interior mean motion resonances J7/2 and J3/1, and Mars exterior mean motion resonances M1/2 and M5/9). Stars indicate the largest member of each family.

independent constraint on the formation age of the Erigone family.

In this paper, we use up-to-date observations and modeling efforts to characterize the Erigone family and revise the collisional evolution of DJ in relation to its membership in the Erigone family. We also discuss predictions for the Lucy mission.

2. Erigone Family: Home of DJ

Analysis of asteroid families, defined as clusters of asteroids on similar orbits as a consequence of high-energy collisions in the main belt, resembles in many respects a journey of discovery to a new land at the dawn of the exploration era. The solitary expedition of this analogy took place more than a century ago (see K. Hirayama 1918), when the largest asteroid families were discovered, namely Themis, Eos, Koronis, and eventually Flora.

Later, when explorers got closer to the new land and their tools improved, additional details were collected and put on maps. In asteroid family research, this phase effectively started in the 1970s and 1980s, when our catalogs of asteroids had substantially grown and mathematical tools needed to define the long-term stable orbital elements of asteroids (the proper elements) had improved.

Thanks to these improvements, the core of what is known today as the Erigone family was discovered by J. G. Williams (1979). At that time, it was simply called family 166 (see also J. G. Williams & J. E. Hierath 1987; J. G. Williams 1992). The cluster only contained a handful of objects and was barely detectable. The discoverer J. G. Williams made an interesting observation, though: that this family resides very close to the Mars-crossing line and could potentially be a source of material leaking into the terrestrial planet region.

The Erigone family is also an interesting case study in how a rapid increase in the number of known asteroids can lead to new challenges. By the 2010s, the number of asteroids with reliably determined proper elements surpassed 10^5, making the limited orbital volume of main-belt space rather crowded. As a consequence, the search for families became an increasingly complicated task. A. Milani et al. (2014) attempted to overcome these challenges using an automated objective scheme of family determination. While the Erigone family is listed in their efforts, these authors do not pay particular attention to it. A more detailed analysis of the Erigone family can be found in F. Spoto et al. (2015), P. Paolicchi et al. (2019), and A. Milani et al. (2019). At first, these authors proposed a split of the Erigone zone into two clusters, called "proper" Erigone and Martes, but they eventually decided that they indeed were a single family.[3] The two extremes of the Erigone family in semimajor axis are in fact produced by the Yarkovsky and Yarkovsky–O'Keefe–Radzievski–Paddack (YORP) dynamical evolution of asteroid family members, as described by D. Vokrouhlický et al. (2006b).

In addition, the Erigone family was shown to have primitive surface materials with a low degree of thermal processing (see A. Cellino et al. 2002; J. R. Masiero et al. 2015, for reviews). Broadband photometry, as well as the detailed spectroscopy of its largest members, indicates that the family belongs to the taxonomic C-type class, while infrared observations show that the Erigone members are low-albedo objects (geometric albedo $p_V < 0.125$). Taken together, the Erigone family belongs to an interesting group of clusters in the inner main belt whose parent bodies were, in all likelihood, implanted in this zone (see review in A. Morbidelli et al. 2015). This region is otherwise dominated by S-type asteroids, akin to ordinary chondrites.

A fundamental aspect of asteroid family studies is how to constrain their formation age. Methods that can help on this front included collisional evolution studies, dynamical considerations, and, exceptionally, crater counts. In this paper, we will focus on the second method, with obvious implications related to the third, as the Lucy mission will return detailed information about DJ's surface.

Dynamical methods of family age determination, which are based on past orbital (and sometimes even rotational) evolution of family members, come in different flavors. For very young families, direct backward orbital propagation of individual orbits allows the user to reconfigure the present-date family structure to the form resulting directly from the collision event producing the family (see reviews in D. Nesvorný et al. 2015;

[3] Curiously, asteroid (5026) Martes, member of the Erigone family, later found its way to family glory by becoming the parent asteroid of an extremely young cluster (see D. Vokrouhlický et al. 2024).

B. Novaković et al. 2022). This approach is only applicable for families with ages less than about 20 Myr.

For older families, the user must rely on techniques having statistical rather than deterministic natures. A popular method is based on identifying and modeling the traces of the Yarkovsky thermal drift in the family structure. The Yarkovsky effect causes asteroids smaller than roughly 30 km in diameter to undergo secular changes in semimajor axis over time (see a review in D. Vokrouhlický et al. 2015). The extent of this process, if analyzed for orbits of members with different size, may constrain the family age. A challenging part of this analysis, however, is to discern the a priori unknown semimajor axis distribution resulting from the initial ejection of fragments with various sizes. Here the YORP effect—a rotational alter ego of the Yarkovsky effect—helps to decorrelate the initial ejection field from the orbital evolution.

Details of the method have been developed in a series of papers by D. Vokrouhlický et al. (2006a, 2006b), with many later variants reviewed in D. Nesvorný et al. (2015). Importantly, D. Vokrouhlický et al. (2006b) found the Erigone family to be an ideal test case for the approach and inferred an age of 280 ± 100 Myr. Subsequent analyses of the Erigone family age with similar or somewhat simplified methods used updated family populations (as the number of detected asteroids in the family steadily increased), with all reaching similar solutions (see W. F. Bottke et al. 2015b; F. Spoto et al. 2015; V. Carruba et al. 2016; B. T. Bolin et al. 2018; P. Paolicchi et al. 2019). The Erigone family was found to be relatively young, with a maximum age of a few hundred Myr.

For the sake of completeness, we also note the work of F. Marzari et al. (1999), who attempted to determine the Erigone family age based on collisional modeling methods. This study was, however, inconclusive. An updated variant of the same technique by M. Brož et al. (2024a) has led to an age of 500 ± 100 Myr. This age is nearly a factor of two older than those obtained from Yarkovsky/YORP orbital solutions, likely due to the uncertainty of their collisional model and its unknown initial conditions. We will make our own collisional modeling calculations for Erigone later in the paper.

In what follows, we take a fresh look at the Erigone family just before Lucy's close encounter with DJ. We will use the most up-to-date catalog of asteroid proper elements provided in D. Nesvorný et al. (2024a), which allows us to investigate Erigone structure to smaller sizes than before. Our goal is also to provide further justification that DJ is a member of the Erigone family, though a definitive proof is impossible owing to the presence of interloping asteroids. Keeping in mind that Lucy's observations will allow us to interpret the nature and history of DJ's surface, we will make an effort to determine a realistic (as opposed to a formal) range of age solutions for the Erigone family.

2.1. A Fresh Look at the Erigone Family

Family identification and morphology in the proper element space. Following closely the method developed by Z. Knežević & A. Milani (2000, 2003), D. Nesvorný et al. (2024a) determined synthetic proper elements for more than a million asteroids in the main belt and made them available through NASA's PDS node[4] (https://pds.nasa.gov/). We applied the Hierarchical Clustering Method (HCM) to this database to search for the Erigone family.

At this stage, we used the traditional variant of the HCM (e.g., V. Zappalà et al. 1990; D. Nesvorný et al. 2015) operating in 3D space of proper semimajor axis a_P, proper eccentricity e_P, and proper sine of inclination $\sin I_P$. We further verified the identified family with color and albedo information at later steps. While the background overdensity of asteroids in the Erigone zone is not a critical problem, some degree of experimentation is needed to fine-tune the HCM velocity cutoff $v_{\rm cut}$. The nominal family realization we shall use here assumes $v_{\rm cut} = 32.5$ m s^{-1}. Smaller values of $v_{\rm cut}$ allow us to identify the family's core, but more distant small members in a halo surrounding the core will be missed. Conversely, large values of $v_{\rm cut}$ associate too many unrelated objects with Erigone. For instance, changing $v_{\rm cut}$ between 28 and 34 m s^{-1} causes the number of members of the cluster to double from 2777 to 5576. After some trial and error, our nominal Erigone family has 4925 members, including DJ.

The top panels of Figure 2 show the projection of the nominal Erigone family onto 2D planes of (a_P, e_P) and (a_P, $\sin I_P$). The bottom left panel shows the proper semimajor axis at the abscissa and the absolute magnitude H on the ordinate. The largest member—Erigone—is approximately at the center of the family. Adopting the reference central value of the semimajor axis $a_c = 2.3695$ au (see below), the $\simeq 2.3 \times 10^{-3}$ au distance of Erigone translates to a transverse velocity kick of $\simeq 10$ m s^{-1} using Gauss equations. This is comfortably smaller than the estimated escape velocity from this asteroid ($\simeq 40$ m s^{-1}). Family asymmetries at this level may be expected if the family was produced from a cratering event on Erigone itself.

The family members extend to both larger and smaller values of a_P, with the smallest members reaching the largest distance from a_c. No strongly chaotic mean motion resonance crosses the Erigone family zone. A few smaller resonances interact with the family, such as the exterior M1/2 resonance with Mars at $\simeq 2.418$ au, the interior J10/3 resonance with Jupiter at $\simeq 2.331$ au, and the three-body resonance (J4,-S2,-1) with Jupiter and Saturn at $\simeq 2.398$ au. They potentially cause some degree of low-level depletion (see D. Nesvorný & A. Morbidelli 1998; A. Morbidelli & D. Nesvorný 1999; T. Gallardo et al. 2011).

The Erigone family belongs to a class of main-belt clusters crossed by high-order secular resonances (see V. Carruba et al. 2018, for review), namely $z_2 = 2(g - g_6) + s - s_6$ in this particular case (see A. Milani & Z. Knežević 1992, 1994, for definition and nomenclature). Erigone members located in z_2, shown by cyan symbols in Figure 2, stretch diagonally in the (a_P, e_P) and (a_P, $\sin I_P$) plots. The strength of z_2 resonance is too small to cause orbital instability, yet its presence in the family zone may have some interesting implications. Asteroids whose semimajor axis is affected by Yarkovsky thermal drift may be captured by z_2 and thereafter follow this resonance (see D. Vokrouhlický & M. Brož 2002, for an example of this phenomenon). We may thus expect some contamination of the Erigone family by interloping objects in the z_2 resonance location.

Finally, due to moderately large e_P values, a potentially destabilizing factor of the Erigone family arises from its location near Mars-crossing orbits at the lowest a_P end (shown approximately by the dashed gray curve in the top left panel of

[4] See also https://www.boulder.swri.edu/~davidn/Proper24 and https://asteroids.on.br/appeal/.

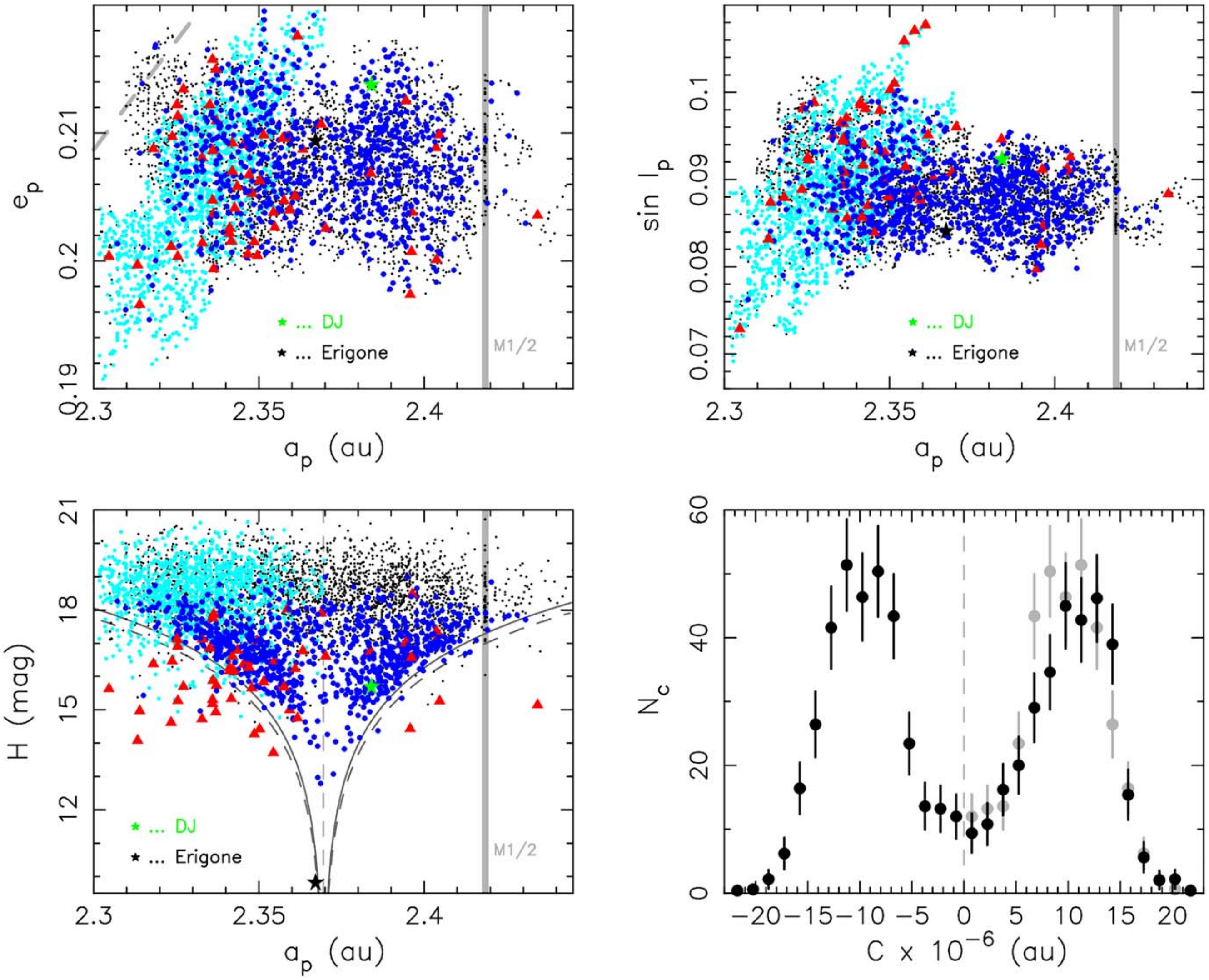

Figure 2. Top panels: Erigone family projected onto 2D planes in proper element space: (i) semimajor axis a_P vs. eccentricity e_P (top left), and (ii) semimajor axis a_P vs. sine of inclination $\sin I_P$ (top right). Black circles are for all 4925 members identified at the HCM cutoff velocity 32.5 m s^{-1}. Color-coded symbols highlight special subgroups of the whole sample: blue circles are 834 low-albedo members ($p_V < 0.125$), red triangles are 55 high-albedo members ($p_V > 0.125$), and cyan circles are members in the z_2 secular resonance (for which $|z_2| < 0.''3\ \mathrm{yr}^{-1}$). The locations of Erigone and DJ are highlighted with black and green stars, respectively. The vertical gray line shows the location of exterior mean motion resonance 1/2 with Mars (M1/2), and the dashed gray curve in the top left panel locates orbits with perihelion $q = 1.82$ au (approximate limit where the population becomes efficiently depleted by Mars encounters). Bottom left panel: Erigone family members projected onto the plane defined by the proper semimajor axis a_P (abscissa) and absolute magnitude H (ordinate). The same color-coding is used as in the top panels. The vertical dashed line shows the center of the family ($a_c = 2.3695$ au), and the two solid gray curves show the limiting $|C_\star| = 1.7 \times 10^{-5}$ au lines defined by maximum conjoint contrast $r(C_\star, a_c; \Delta C)$ (see Equations (1) and (A3)), while the dashed gray curves correspond to $|C_{\rm fam}| = 1.95 \times 10^{-5}$ au, the limit used for Yarkovsky/YORP chronology modeling. Formal members with H smaller than $H_\star$ at the critical lines, for a given a_P value, are deemed unrelated interlopers in the family. Bottom right: distribution of $H \leqslant 17.5$ mag Erigone members $dN(C)$ with $|C| \leqslant C_{\rm fam}$ values binned with $\Delta C = 1.5 \times 10^{-6}$ au intervals; only WISE-identified dark asteroids are used in this data set. The black symbols, with formally adopted $\sigma(C) = \sqrt{dN(C)}$ uncertainty, are raw data. The gray symbols at $C \geqslant 0$ values mirror the $C \leqslant 0$ distribution.

Figure 2). A fraction of the Erigone population with $H \geqslant 18$ might have leaked (and is also currently leaking) to the terrestrial planet zone (given their low albedo values, these are $\lesssim$1.4 km dark asteroids). As also shown in the top left panel of Figure 2, z_2 resonance captures may help decrease this flux into the Mars-crossing region.

Erigone family in the semimajor axis versus absolute magnitude projection. Erigone family members are distributed in the (a_P, H) plane in a pattern characteristic of other families: the largest objects are located near the center, smaller members with diameter D are dispersed from the center up to a distance roughly proportional to D^{-1}. At first glance, this may look like the signature of the fragments' ejection velocity field at the moment of family formation. A closer analysis, however, reveals that this contribution must only be a small fraction of the total. The reasons are as follows.

First, the equivalent velocities required to explain the observed-family extension are far larger than the escape velocity from the parent asteroid (e.g., A. Cellino et al. 2004). Second, the distribution of $H \leqslant 18$ members in the (a_P, H) plane avoids the center of the family and instead exhibits a peculiar polarization toward the extreme largest and smallest a_P values. The latter property is not compatible with any reasonable ejection velocity field. It only makes sense as a consequence of long-term orbital evolution driven by the synergy of the Yarkovsky and YORP effects (the latter assisting the former by tilting spin axes to the direction normal to the orbital plane; see D. Vokrouhlický et al. 2006b). Erigone is in fact an exemplary case that is well suited for age dating via our Yarkovsky/YORP chronology model. We shall apply it to the new nominal realization in what follows.

It is worth mentioning that this polarization pattern disappears for $H > 18$ members. This observation does not contradict the Yarkovsky/YORP model; rather, it is an expected prediction. As discussed by W. F. Bottke et al. (2015b), these small members experience such fast YORP evolution that, depending on the family's age, they undergo a large number of so-called "YORP cycles." A YORP cycle is defined as a case where an asteroid goes from a generic initial spin vector state to an asymptotic YORP end state. Examples of the latter include the body spinning so fast that its sheds mass (and changes shape) or so slowly that it enters into a tumbling rotation state. When the asteroid emerges from this YORP end state, the pattern begins again, with the body once again spinning up or down toward a YORP end state. As a result, asteroids that undergo many YORP cycles do not continue their steady push toward the most extreme values of a_P, but instead evolve via a random walk. This causes small family members to take a characteristic Gaussian-type distribution of proper semimajor axis. We note that this concept was developed more fully by P. Paolicchi & Z. Knežević (2016) and P. Paolicchi et al. (2019) and that these papers also include a discussion of the Erigone family.

Accordingly, our Yarkovsky/YORP model of moderately young families, including Erigone, must account for the spin vector evolution of their members. Transport of small members toward extremely large or extremely small values of a_P by the Yarkovsky effect requires prograde or retrograde rotation states, respectively. This prediction has recently been tested in the case of several families by J. Ďurech & J. Hanuš (2023), with the results matching expectations. In the case of the Erigone family, the available spin state solutions are unfortunately somewhat limited. We review the current situation in Appendix A.3.

Albedo data and C*-foliation of the* (a_P, H) *space*. Further justification of the identified nominal Erigone family arises from the available observations at infrared wavelengths, as well as visible multicolor photometry (see A. Parker et al. 2008; J. R. Masiero et al. 2011, 2013). Here we use data obtained by the Wide-field Infrared Survey Explorer (WISE; J. R. Masiero et al. 2011) that provided diameter and albedo values for more than 125,000 asteroids. J. R. Masiero et al. (2015) used the 2015 edition of the PDS family identification (D. Nesvorný et al. 2015) and identified 716 Erigone members with WISE data. They determined the predominance of dark-albedo objects, with a median albedo of 0.05 ± 0.01 (this is in agreement with color indices obtained using observations of the Sloan Digital Sky Survey (SDSS) being compatible with predominant C-complex taxonomy; e.g., A. Parker et al. 2008; J. R. Masiero et al. 2015; D. Morate et al. 2016; B. Harvison et al. 2024).

Our nominal Erigone family contains 889 members for which WISE provides size and albedo values. The albedo distribution of members of the Erigone family shows a high-albedo tail that becomes discontinuous for albedos greater than 0.125. Figure 3 shows the distribution of the geometric albedo values p_V of this sample. The albedo limit at $p_V^\star$ (shown by the red dashed line) clearly terminates the bulk of the dark population. Thus, adopting the albedo value of $p_V^\star = 0.125$ as a criterion to divide the sample into dark objects (defined here as low albedo) and bright objects (defined here as high albedo), we find 834 dark members and 55 bright members (the WISE sample in the family is highlighted by blue circles (dark members) and red triangles (bright members) in Figure 2). The median albedo of the dark sample is $\bar{p}_V = 0.054$, very close to the results of J. R. Masiero et al. (2013, 2015).

Overall, the bright interlopers only represent 6.1% of the nominal family. Restricting ourselves to the (a_P, H) region within the two dashed gray lines shown in the bottom left panel of Figure 2, we find that the population of dark members is 828 and the sample of bright interlopers drops to 34 (representing now only 3.9%). Likewise, the region outside the two dashed gray lines contains only six dark objects but 17 bright ones. Furthermore, these "exterior" bright interlopers mostly have $a_P \leqslant 2.35$ au; they show an affinity to the orbital location of the z_2 secular resonance. This supports our suspicion that a significant fraction of the low-level contamination of the Erigone family may be associated with interlopers migrating along this resonance (possibly over a Gyr). These objects would therefore sample various parts in the inner main belt. This justifies our decision to restrict our further analysis to a subsample of the nominal Erigone family delimited in the (a_P, H) plane by the interior of the dashed gray lines. This approach has been adopted by many previous studies and was reviewed in Section 4 of D. Nesvorný et al. (2015). In Appendix A.1 we provide a method to quantitatively determine the family formal center a_c and its borderline gray lines shown in Figure 2.

In order to further analyze the Erigone family, we need to define our notation and variables for our Yarkovsky/YORP chronology model. Here we introduce a method of folding data in the 2D (a_P, H) plane onto a suitable 1D variable (see D. Vokrouhlický et al. 2006b, for more details). To that end, we define parameter C using an implicit relation

$$H(C, a_P; a_c) = 5\log\left(\frac{a_P - a_c}{C}\right), \tag{1}$$

where a_c is a free parameter of symmetry: given a certain value of H, positive and negative values of C correspond to a_P values symmetric with respect to a_c. In the case of the Erigone family we adopt $a_c = 2.3695$ au (see Appendix A.1 for a formal method that justifies this value).

The relevance of the C parameter for our Yarkovsky model consists of the fact that asteroids starting at a_c (or very close) and maintaining a constant drift rate of da_P/dt would, in a given time T, reach the same C-isoline independently of their size D. The reason is because $da_P/dt \propto D^{-1}$. Asteroids drifting at the maximum possible Yarkovsky rate, namely those having extreme obliquity values of 0° or 180°, would reach a maximum isoline $|C_{\rm fam}| = (da/dt)_{1329}\sqrt{p_V}\, T$ (e.g., D. Vokrouhlický et al. 2006b; D. Nesvorný et al. 2015; here $(da/dt)_{1329}$ is the drift rate of a $D = 1329$ km large asteroid). This "wave front" of asteroids is close to the gray lines shown in the bottom left panel of Figure 2, which are in fact defined by Equation (1) for a certain C values.

With C defined, we can now represent the family population using a distribution $\mathcal{D}(C)$, such that the number of family members between $(C, C + dC)$ is $dN(C) = \mathcal{D}(C)\,dC$. The black symbols in the bottom right panel of Figure 2 show dN values for bins $dC = 1.5 \times 10^{-6}$ au that are restricted to (i) Erigone members with dark albedo values by WISE ($p_V \leqslant 0.125$) and (ii) those having $H \leqslant 17.5$. The first condition

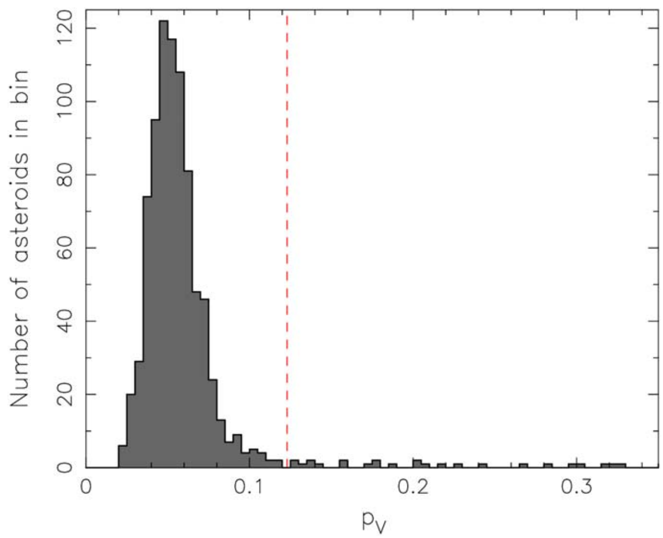

Figure 3. Distribution of the geometric albedo values p_V for 862 members in the Erigone family delimited by the dashed gray curves in the (a_P, H) shown in Figure 2 (the ordinate is a number of asteroids in 0.005 wide albedo bins). The bulk of the family asteroids have dark albedo values with $p_V \leqslant p_V^\star = 0.125$ (red dashed line) confined in a narrow peak about the median $\bar{p}_V = 0.054$, followed by a tail subpopulation with p_V values terminated by $p_V^\star$ (see also J. R. Masiero et al. 2013). No clustering of p_V values is seen above $p_V^\star$ among a group of 34 bright objects, suggesting that they are interlopers in the family.

should minimize contamination by interlopers, while the latter is given by our intention to use these data for the Yarkovsky/YORP chronology of the Erigone family. We use the latter because the $H \leqslant 17.5$ population shows the optimum telltale signature of Yarkovsky/YORP synergy over the family age. The family members pile up to the a_P values along the above-defined $C_{\rm fam}$ isoline and deplete the center of the family. As discussed above, the population of smaller members with $H > 17.5$ falls into a different Yarkovsky/YORP regime, when T is large compared to the timescale of YORP cycles and asteroid orbits perform a random walk in a_P rather than steady flow. We avoid using this regime for family chronology, since modeling repeated YORP cycles is challenging given our current state of knowledge.

The $dN(C)$ distribution shown in Figure 2 shows distinct maxima at $C_{\rm max} \simeq \pm 1.1 \times 10^{-5}$ au and a minimum in the center. This reflects the concentrations of the Erigone members at the extreme a_P values for a given H in the (a_P, H) plane. For an optimum choice of a_c, the distribution $dN(C)$ should be nearly symmetrical in C. This claim can be visually tested by the gray symbols, which just flip the distribution with negative C to their symmetric positive C values. While not completely symmetric, the degree of symmetry is deemed satisfactory for our work (the observed difference may be due to a slight anisotropy of the initial ejection velocity field or interloper contamination in the $a_P \leqslant 2.35$ au). Given that we do not intend to model such details, we shall use a fictitious distribution

$$dN_{\rm sym}(C) = \frac{1}{2}[dN(C) + dN(-C)], \tag{2}$$

with an enforced symmetry for our Yarkovsky/YORP chronology model.

Size distribution of Erigone family members. The left panels of Figure 4 show albedo and size data for 889 Erigone family members determined using WISE observations (J. R. Masiero et al. 2011, 2013): (i) albedo values with their uncertainty (top left), and (ii) cumulative size distribution (bottom left). In the case of multiple inputs for a given body, we first drop data with too few observations in the W3 passband (namely fewer than six) and take the average albedo value from the remaining set. Interestingly, the largest members with $D > 10$ km have albedo values smaller than the median $\bar{p}_V = 0.054$ of the whole sample of dark objects. This could suggest a slight trend toward higher albedos for small members. More likely, there is some unrecognized systematic component in the uncertainty for these small asteroids. In fact, the case of DJ with $p_V = 0.103 \pm 0.019$ may be an exemplary case, as we argue below.

As for the size distribution shown in the bottom part of the plot, we show the size–frequency distributions (SFDs) of 834 dark objects provided by WISE observations (blue curve) and those for 4925 members in the nominal family. For the latter, we assign to all objects the median albedo value 0.054 (and using their Minor Planet Center absolute magnitude values; red curve). The difference between the two SFDs is small but noticeable. It arises from the lower albedo values of the Erigone family's largest members. This mismatch illustrates the uncertainty in other asteroid family studies that infer the family's SFD from the absolute magnitude distribution data while also assuming that the family albedos correspond to the taxonomic class of the largest members.

Finally, the right panel of Figure 4 shows the $dN(C)$ distribution for Erigone family members with $H \leqslant 17.5$ (in Appendix A.2 we argue that this sample in complete). For reference, we repeat the distribution for the 640 dark members with $|C| \leqslant C_{\rm fam}$ from Figure 2 (blue symbols), while the red symbols show the whole Erigone sample. The two distributions are similar to each other. Multiplying the former by a factor 1.9 allows one to obtain an excellent match to the latter (this is shown by the black line). This confirms that there are few interloping objects in either sample of Erigone family members. In fact, the factor 1.9 is a good estimate of incompleteness for WISE asteroid observations with $H \leqslant 17.5$ in the Erigone zone. This incompleteness does not stem from photometric sensitivity of WISE, as the fluxes in its W3 passband should correspond to the IR equivalent magnitude $\lesssim 10.25$ (the limit of the instrument; e.g., A. Mainzer et al. 2011). Instead, it stems from some Erigone members that did not happen to geometrically fit in the WISE field of view. The growing mismatch beyond the family limit in the $C < -20 \times 10^{-6}$ au bins is likely an expression of the interloper population located in the z_2 secular resonance (see Figure 2).

Yarkovsky/YORP chronology revisited. We now revisit our determination of the Erigone family age T using the Yarkovsky/YORP method. The general outline of our approach is given in Appendix A.4. More details can also be found in D. Vokrouhlický et al. (2006b) and W. F. Bottke et al. (2015b). The goal is to match the family distribution $dN_{\rm sym}(C)$ in the C parameter using a suitable model prediction $dM(C; \boldsymbol{p})$. The model performance is evaluated using a target function

$$\chi^2 = \sum_i \left(\frac{dN_{{\rm sym},i} - dM_i(\boldsymbol{p})}{\sigma_i} \right)^2, \tag{3}$$

where $\sigma_i = \sqrt{dN_{{\rm sym},i}}$ and the summation runs over $|C| \leqslant C_{\rm fam}$ bins. The formal confidence boundary of the parameter solution stems from the dimensionality of the $\boldsymbol{p}$-space. With six parameters used, our 90% confidence level corresponds to a hyperspace delimited by a $\delta\chi^2 = 10.6$ increase of the target function over the best-fit value (e.g., W. H. Press et al. 2007).

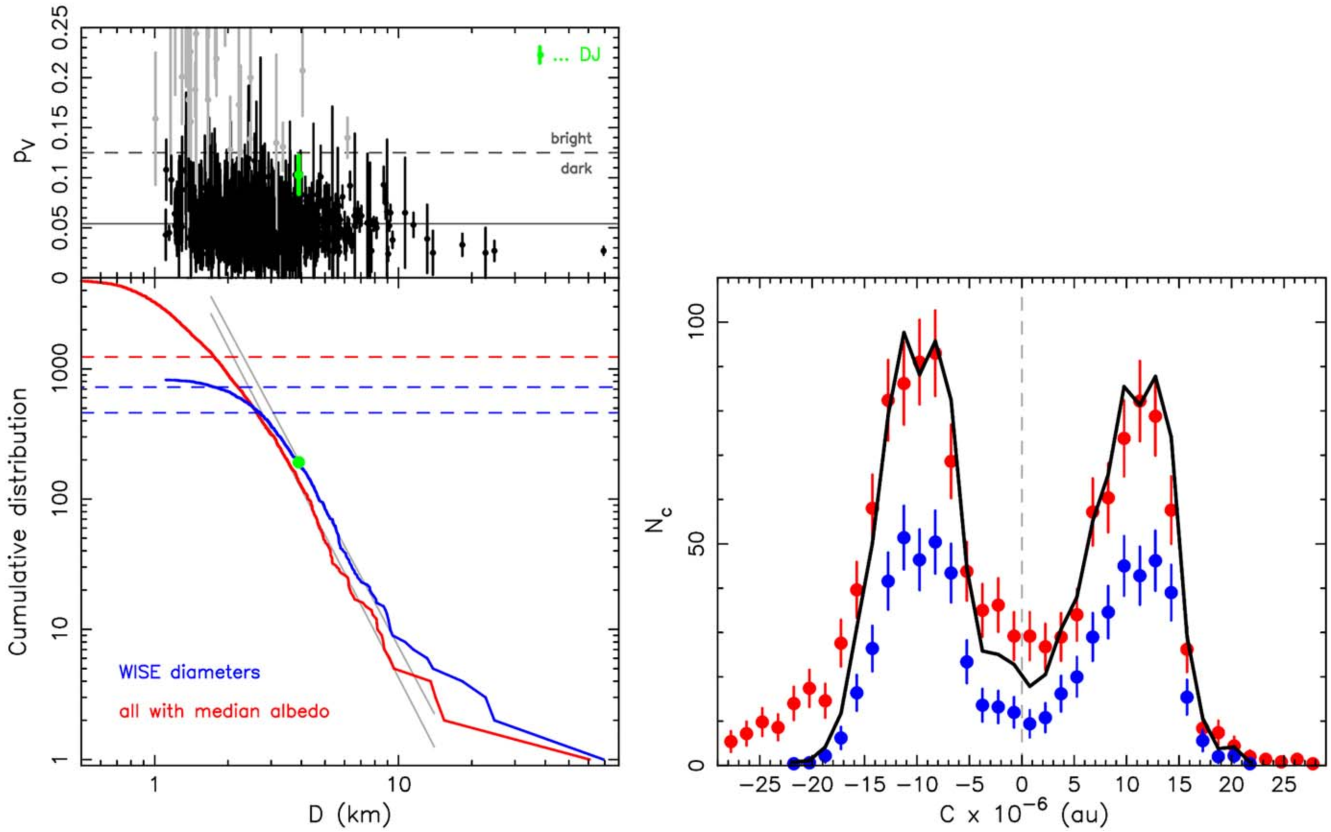

Figure 4. Top left: geometric albedo values p_V, with formal uncertainties, determined for 889 Erigone family members by analysis of WISE observations. The sample is dominated by 834 dark objects ($p_V < 0.125$) shown by black symbols. The albedo values for a bright group (55 objects with $p_V > 0.125$) are shown using gray symbols (some would fall even beyond the upper limit 0.25 of the plot). DJ's value is shown in green. The horizontal gray line at $\bar{p}_V = 0.054$ indicates the median value of the dark sample. Note that the largest objects ($D > 10$ km) have systematically $p_V < \bar{p}_V$. Bottom left: cumulative size distribution of Erigone family members; the red curve is for all 4925 members assigning to all median WISE albedo $\bar{p}_V = 0.054$ for the dark sample and adopting their absolute magnitudes, and the blue curve is for the distribution of size for 834 members with WISE dark albedo. DJ's location is marked by the green symbol. The gray lines are approximations with power-law distribution $N(>D) \propto D^{-\alpha}$ in the 4–10 km range, with $\alpha \simeq 3.63$ for the whole population (red) and $\alpha \simeq 3.50$ for the WISE subsample (blue). The horizontal dashed lines correspond to the $H = 17.5$ mag limit. This is unique for the whole sample in red (where sizes are computed from magnitudes using a fixed albedo value), while $H = 17.5$ asteroids are in a certain range in the WISE sample, because individual objects have slightly different p_V values. Right panel: distribution of $dN(C)$ binned with $\Delta C = 1.5 \times 10^{-6}$ au intervals for $H \leqslant 17.5$ mag Erigone members (formal $\sqrt{dN(C)}$ uncertainties shown by the vertical bar); the blue symbols are for the subsample of asteroids with WISE-determined $p_V < 0.125$ albedo values and $|C| \leqslant C_{\rm fam}$ (the same as the black symbols in the bottom right panel of Figure 2), and the red symbols are for all Erigone members. The black line is simply the blue distribution multiplied by a factor 1.9. A good match to the total population suggests (i) a small fraction of bright interlopers in the Erigone family up to the $H = 17.5$ mag limit and (ii) that there is a 1.9 incompleteness factor of the WISE-observed sample. The mismatch for $C < -20 \times 10^{-5}$ au is likely due to contamination by bright objects transported along the z_2 secular resonance.

As for the parameters $\boldsymbol{p}$, we split them into two groups: $\boldsymbol{p} = (\boldsymbol{p}_1; \boldsymbol{p}_2) = (T, v_5, c_{\rm YORP}; \rho, \Gamma, \tau_0)$. The first set, $\boldsymbol{p}_1$, has been considered already by D. Vokrouhlický et al. (2006b). It consists of (i) the family's age T, (ii) the initial ejection velocity v_5 of $D = 5$ km fragments (assuming the ejection velocity v_5 $(5\,{\rm km}/D)$ of fragments with an arbitrary diameter D), and (iii) a scaling factor $c_{\rm YORP}$ of the reference YORP torque taken from D. Čapek & D. Vokrouhlický (2004). In the production simulations, we sampled the following range of these parameters: 50–500 Myr for T, 0–50 m s^{-1} for v_5, and 0–2 for $c_{\rm YORP}$.

The second set, $\boldsymbol{p}_2$, consists of (i) the bulk density ρ of the Erigone family members, (ii) their surface thermal inertia Γ, and (iii) the characteristic timescale τ_0 of the YORP strength modification for $D = 1$ km members (assuming that its size dependence is $\propto \tau_0 \sqrt{D/(1\,{\rm km})}$). The last parameter corresponds to what W. F. Bottke et al. (2015b) called variable or stochastic YORP. This concept arises from the fact that YORP torques have a substantial dependence on the small-scale irregularities of an asteroid's shape. As a result, asteroid shape changes caused by subcatastrophic impacts or landslides may change the strength of YORP torques for kilometer-size asteroids. The role of these parameters on age calculations has yet to be fully evaluated, and in some cases it could be meaningful.

Here we consider τ_0 in the 0.5–100 Myr range. Concerning the bulk density and surface thermal inertia, we will use observed parameters for Bennu and Ryugu because these bodies are thought to be close analogs of what we might expect for Erigone kilometer-size family members. Bennu's mean bulk density was found to be 1.2 g cm^{-3} (e.g., D. S. Lauretta et al. 2019; D. J. Scheeres et al. 2020), while its mean surface thermal inertia was 300 ± 30 J m^{-2} K^{-1} s$^{-1/2}$ (denoted SI units below for short; B. Rozitis et al. 2020). Given that specific regions of Bennu, such as its equatorial ridge zones, were found to be modestly lower in density, slightly higher bulk density values may also be possible. Similarly, specific fine-grained locations or an anomalous rock population (likely covered with fine dust layer) on Bennu's surface have thermal inertia values as low as $\simeq 150-200$ SI units. The larger heliocentric distance of Erigone family members, which means lower mean temperatures, may make it worthwhile to explore these lower thermal inertia values.

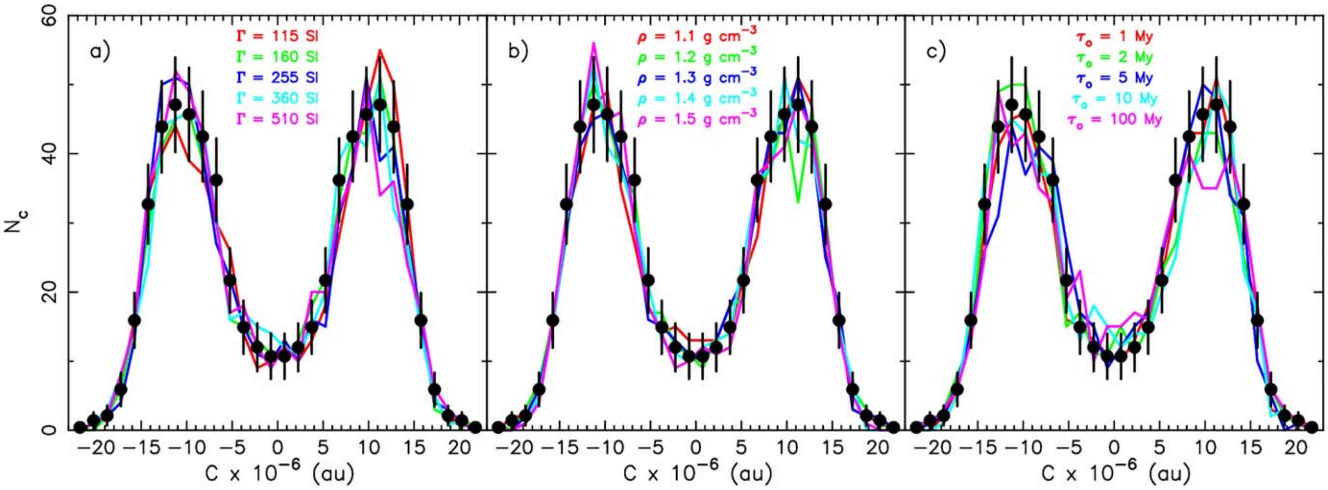

Figure 5. Best-fit solutions from a set of trial simulations sampling each time only one of the parameters $\boldsymbol{p}_2 = (\rho, \Gamma, \tau_0)$ in our model: (i) fixed values $\rho = 1.3$ g cm^{-3} and $\tau_0 = 1$ Myr with five values of Γ listed in labels and color (left panel), (ii) fixed values $\Gamma = 160$ SI and $\tau_0 = 1$ Myr with five values of ρ listed in labels and color (middle panel), and (iii) fixed values $\rho = 1.3$ g cm^{-3} and $\Gamma = 160$ SI with five values of $\tau_0 = 1$ Myr listed in labels and color (right panel). The black symbols with uncertainty intervals show the data, namely distribution $dN_{\rm sym}(C)$ (Equation (2)), with $|C| \leqslant C_{\rm fam}$ values binned using $\Delta C = 1.5 \times 10^{-6}$ au intervals for $H \leqslant 17.5$ mag Erigone members with WISE dark albedo values. In each case the solution is statistically acceptable, indicating correlations between the parameters. In simulations (i) and (ii), the left and middle panels, the Erigone age T approximately scales with the tested parameter, i.e., $T \propto \Gamma$ and $T \propto \rho$ as expected from analytic formulae for da/dt (e.g., D. Vokrouhlický et al. 2015). In the last simulation (iii), the right panel, T depends on τ_0 only weakly, but the χ^2 value increases for larger τ_0.

Ryugu studies show that it also has a mean bulk density of 1.2 g cm^{-3} (e.g., S. Watanabe et al. 2019) and a surface thermal inertia close to 300 SI units (e.g., T. Okada et al. 2020). We note that some studies report lower values such as $\Gamma = 225 \pm 45$ SI units in Y. Shimaki et al. (2020). On the other hand, possible meteorite analogs of Erigone family members (CM or CR chondrites; e.g., M. Brož et al. 2024a) often have larger densities and thermal inertia values. We caution that these objects probably represent a biased sample; weaker objects may be unable to survive passage through Earth's atmosphere. Still, rather than limit ourselves in our runs, we opted to explore bulk density values in the range 1.2–1.7 g cm^{-3} and surface thermal inertia in the 100–650 SI units range. For the sake of simplicity, we do not account for any possible size dependence on thermal inertia for this study (see B. T. Bolin et al. 2018, for discussion and results).

Before discussing results from the suite of production simulations, where we sample the entire 6D parameter space of our model, we first ran a set of trial simulations. Here we tested the dependence of the results on each of the $\boldsymbol{p}_2$ parameters individually (but taking into account the $\boldsymbol{p}_1$ parameters over their range). Results are shown in Figure 5. In each of the trial simulations, we find a statistically acceptable solution. This hints that parameter correlations exits, which in fact is expected.

In the left and middle panels, we confirm the Erigone age scalings $T \propto \rho$ and $T \propto \Gamma$ that follow from the corresponding inverse scaling of the Yarkovsky drift rate da/dt (the latter due to the predominant larger thermal parameter regime; e.g., D. Vokrouhlický et al. 2015). Therefore, younger ages are obtained for the Erigone family provided that densities and/or thermal inertia values are small (or some combination of the two). Likewise, older family ages come from larger densities and/or thermal inertia values (or some combination of the two).

We find that the age does not depend strongly on the τ_0 value, but $\tau_0 > 50$ Myr does provide poorer fits to the observational data. The reason is because there is a significant contrast between the maximum of $dN_{\rm sym}(C)$ at $C_{\rm max} \simeq 1.1 \times 10^{-5}$ au at the family center $C = 0$. It requires the evolution of the rotation rates to be delayed compared to obliquities via the YORP effect. This behavior is well represented by the random walk effect in rotation rate provided by variable YORP (see, e.g., the Appendix in W. F. Bottke et al. 2015b).

Figure 6 shows results from our production simulations. We focus here on the solution for the age of the Erigone family. The formal best-fit solution with $\chi^2 = 6.46$ corresponds to the following set of parameters: $\rho = 1.5$ g cm^{-3}, $\Gamma = 135$ SI, $\tau_0 = 0.6$ Myr, $T = 155$ Myr, $v_5 = 24$ m s^{-1}, and $c_{\rm YORP} = 1.5$. We caution that because there are multiple correlations, the admissible range of solutions is arguably more important than the best-fit solution. Using the 90% confidence level limit, we projected its volume in 6D $\boldsymbol{p}$-space onto the 1D distribution of the family age T. These values are shown in the top panel of Figure 6. The median age $\bar{T} = 186$ Myr with an asymmetric C distribution. The youngest age is $\approx$115 Myr, while the oldest ages extend to 350 Myr owing to a stretched tail.

To understand this behavior, we broke the distribution into six categories in density, as shown by the color histograms in the top panel of Figure 6. Apart from the obvious $T \propto \rho$ scaling, there is a self-similarity that takes place, as the individual distributions correspond to various density values. The long tails correspond to simulations with large thermal inertia values (Γ). This result is confirmed in the bottom panel of Figure 6, where we show the 90% confidence level age distribution for a fixed value $\rho = 1.3$ g cm^{-3}: the color distributions break the simulations into different Γ values for various intervals. As anticipated, the age solutions larger than $\simeq$250 Myr are in the long tail and are obtained for large Γ values.

Finally, we ran checks to make sure that the parameter set $\boldsymbol{p}$ of our solutions does not contradict the Erigone family structure in the (a_P, H) plane for $H \geqslant 18$ (bottom left panel of Figure 2). The Yarkovsky/YORP model is based on matching the polarization of $H \leqslant 17.5$ members in a_P toward "extreme" values defining the $C_\star$ isoline. This behavior is not observed in the Erigone $H \geqslant 18$ population, so the accepted solutions must satisfy this constraint.

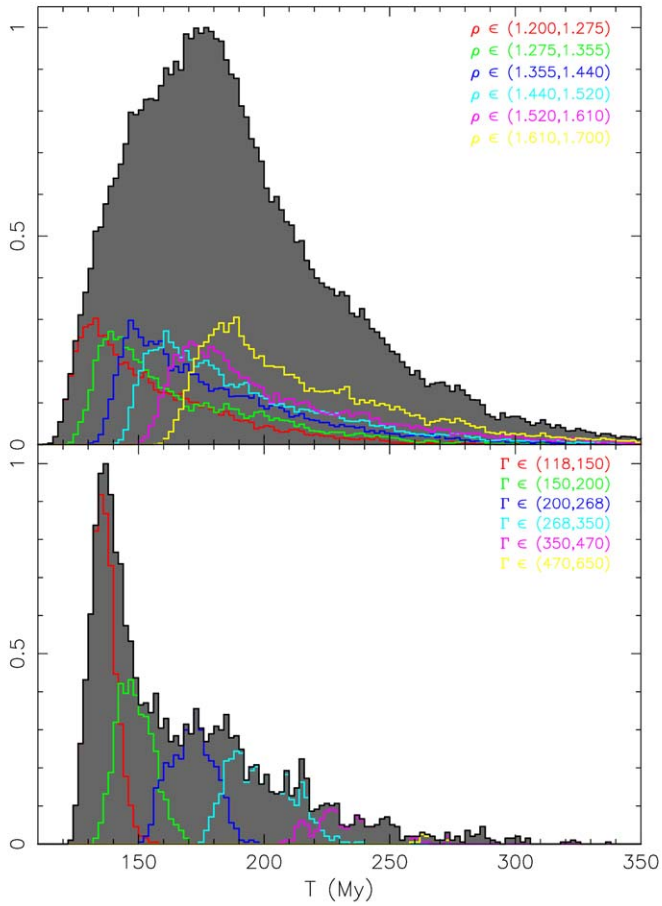

Figure 6. Top panel: distribution of the Erigone family age T from a set of simulations in which all parameters $\boldsymbol{p}_2 = (\rho, \Gamma, \tau_0)$ uniformly sampled the following interval of values (gray histogram with black outline): (i) $\rho \in (1.2, 1.7)$ g cm^{-3}, (ii) $\Gamma \in (115, 710)$ SI, and (iii) $\tau_0 \in (0.5, 100)$ Myr (the last two in log-measure). The median age is 186 Myr. The color-coded distributions are for subsamples characterized by distinct bulk densities: (i) $\rho \in (1.2, 1.275)$ g cm^{-3} (red), (ii) $\rho \in (1.275, 1.355)$ g cm^{-3} (green), (iii) $\rho \in (1.355, 1.44)$ g cm^{-3} (blue), (iv) $\rho \in (1.44, 1.52)$ g cm^{-3} (cyan), (v) $\rho \in (1.52, 1.61)$ g cm^{-3} (magenta), and (vi) $\rho \in (1.61, 1.7)$ g cm^{-3} (yellow). All distributions are normalized by the maximum of the total distribution. The lower-density solutions imply a smaller family age. Bottom panel: distribution of the Erigone family age T from a set of simulations in which bulk density was fixed to 1.3 g cm^{-3}, but with the remaining two parameters $\boldsymbol{p}_2 = (1.3, \Gamma, \tau_0)$ sampling the following interval of values (gray histogram with black outline): (i) $\Gamma \in (118, 650)$ SI, and (ii) $\tau_0 \in (0.5, 100)$ Myr (both in log-measure). The color-coded distributions are for subsamples characterized by distinct values of the thermal inertia (all in SI units): (i) $\Gamma \in (115, 150)$ (red), (ii) $\Gamma \in (150, 200)$ (green), (iii) $\Gamma \in (200, 268)$ (blue), (iv) $\Gamma \in (268, 350)$ (cyan), (v) $\Gamma \in (350, 470)$ (magenta), and (vi) $\Gamma \in (470, 650)$ (yellow). The lower-inertia solutions imply a smaller family age. As demonstrated by the two panels, the family age becomes more constrained if one or more parameters are determined.

We ran the Yarkovsky/YORP model with the best-fitting set of parameters $\boldsymbol{p}$ mentioned above. For each time, we took a synthetic (not real) population of 640 asteroids of a fixed magnitude H, sampling values from 16 to 19 with an increment of 0.5 (their sizes were derived from the standard magnitude–size relation assuming the median albedo value 0.054 of the family members). We ran the model for $T = 155$ Myr and determined the final $dM(C; \boldsymbol{p})$ distribution for each magnitude class separately. The results are shown in Figure 7.

The simulations that propagated $H \leqslant 17.5$ asteroids provided the double-peak distribution needed to match the data (shown with light-gray symbols for completeness). Moving to results in simulations where $H \geqslant 18$, the resulting distribution changes, having just a single maximum at the family center. As discussed above, this behavior follows from the asteroids performing a random walk in a_P owing to short YORP cycles instead of a steady flow toward the $C_\star$ limit. While our fits are satisfactory, we caution the reader that proper modeling of this evolutionary regime is difficult with our approximate model. For that reason, we do not use it in determining the family's age.

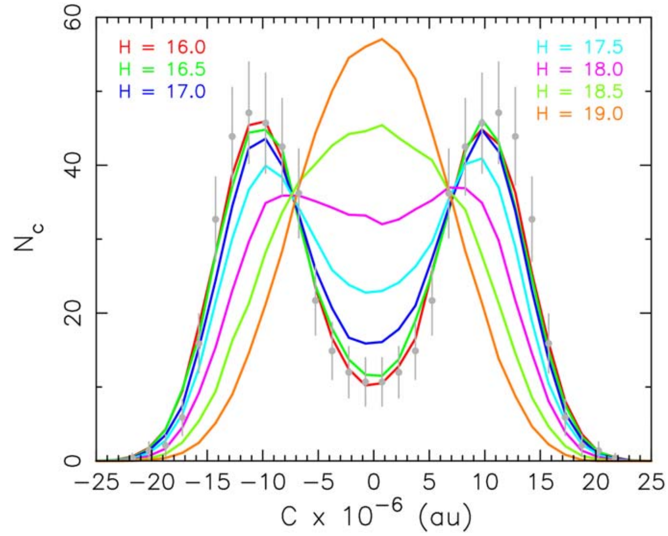

Figure 7. Model prediction of the C parameter distribution $dM(C; \boldsymbol{p})$ determined from test simulations, in which all asteroids were given the same absolute magnitude value H (color-coded with labels) and the parameters $\boldsymbol{p}$ were the best-fit set from the Yarkovsky/YORP chronology method. The latter used only $H \leqslant 17.5$ Erigone dark members with their WISE-determined sizes. Here in each magnitude class we assigned sizes from H and 0.054 albedo value, and we pushed the tested H values beyond the 17.5 limit. In the simulations with $H \leqslant 17.5$ we recover the two-hump $dM(C; \boldsymbol{p})$ distribution fitting the data (gray symbols), but runs with $H \geqslant 17.5$ result in a single-peaked $dM(C; \boldsymbol{p})$ distribution due to asteroids performing a random walk in a_P related to a quickly decreasing YORP cycle timescale with size. This transition at approximately 1 km size is indeed seen in the distribution of family members in the (a_P, H) plane (bottom left panel of Figure 2).

Size of Erigone family parent body. One of the more challenging aspects of asteroid family studies is estimating the original size of the parent body. The reason is that in a family-forming event a considerable amount of mass is placed into fragments that are smaller than the observation limit in the main belt (e.g., D. D. Durda et al. 2007), which is probably near a few kilometers in diameter. Even if we could somehow magically see all of this material in the present day, we would still have issues because subkilometer objects are readily ground down over hundreds of Myr by collisional processes (e.g., W. F. Bottke et al. 2015a).

One way to get around this problem is to consider the largest members of a family. They are the least affected by collisional evolution and typically have very slow Yarkovsky drift rates. The combination implies that these bodies are probably the most unchanged within a family. Accordingly, these bodies can be compared to the SFDs of results from numerical hydrocode simulations of impacts. Specifically, here we will make comparisons to the 161 simulations conducted to study asteroid satellite formation by D. D. Durda et al. (2004). Numerical impact simulations must conserve mass, so if we can find a match between a scaled version of a model-family SFD and the observed-family SFD for the largest fragments, the results can give us insights into the initial parent body size. Our method is as follows.

First, our collisional results from D. D. Durda et al. (2004) were obtained by tracking the results of impacts between two asteroids using the three-dimensional smoothed particle hydrodynamics (SPH) code SPH3D (W. Benz & E. Asphaug 1994). Computational details of these simulations can be found in D. D. Durda et al. (2004, 2007). Once the ejecta flow field from the impacts is established, the results were handed off to the *N*-body code `pkdgrav` (e.g., Z. M. Leinhardt et al. 2000; D. C. Richardson et al. 2000; J. G. Stadel 2001; Z. M. Leinhardt & D. C. Richardson 2002). `pkdgrav` is a scalable, parallel tree code for modeling the gravitational interactions between the resulting fragments. It has the ability to detect and treat low-speed collisions between particles and allows rubble-pile accumulations to form among ejected fragments.

The target asteroids from D. D. Durda et al. (2004) were 100 km diameter undamaged basalt spheres. The spherical basalt projectiles had diameters of 10–46 km (10, 14, 18, 25, 34, and 46 km), impact speeds from 2.5 to 7 km s^{-1}, and impact angles ranging from 15° to 75° (i.e., nearly head-on to very oblique). Details of the simulation outcomes are presented in Table 1 of D. D. Durda et al. (2004). We note that Erigone is a carbonaceous chondrite asteroid and therefore may not be a good match to the target properties of basalt. On the other hand, numerical impact experiments show that carbonaceous-chondrite-like bodies, with lower densities but higher porosities than ordinary-chondrite-like bodies, require similar collisional energies to produce catastrophic disruption events (e.g., M. Jutzi et al. 2015). Given that our work is mainly an attempt to glean insight into the size of the Erigone parent body, we will stick to using the D. D. Durda et al. (2007) results for now. Future work after Lucy's encounter with DJ can revisit this issue when more is known about the physical properties of DJ.

There are two observed SFDs for the Erigone family shown in the bottom left panel of Figure 4. One uses WISE diameters (blue line), while the other converts the absolute magnitude of Erigone family members into diameters using the family's median albedo. We tested both using the fitting procedure discussed in D. D. Durda et al. (2007). Our primary diagnostic values are the diameter ratio of the largest and the second-largest remnants and the shape of the continuum SFD for bodies smaller than the second-largest remnant. The model SFDs were scaled to match these values as best as possible, with the scaling factor telling us how much larger or smaller the parent body was likely to be than the starting size of 100 km.

Curiously, we were unable to find any satisfying fits to the WISE-diameter SFD using the D. D. Durda et al. (2007) model (Figure 8). We suspect that this is because the largest two bodies have irregular shapes, making their WISE diameters less representative of their true diameters than one would expect. It could also be that the physical properties of basalt are not a good proxy for how carbonaceous-chondrite-like material behaves in a disruptive collision. More work is needed to better understand this issue.

For the other Erigone family SFD based on the absolute magnitude of the family members and the family's median albedo, we found two reasonable fits to the D. D. Durda et al. (2004) results. They are defined as "Basalt_5_45_1.8" and "Basalt_6_30_2.2." Both are shown in Figure 8 and can also be found in Figure 3 of D. D. Durda et al. (2007). The suffixes in the runs correspond to impact velocity, impact angle, and the

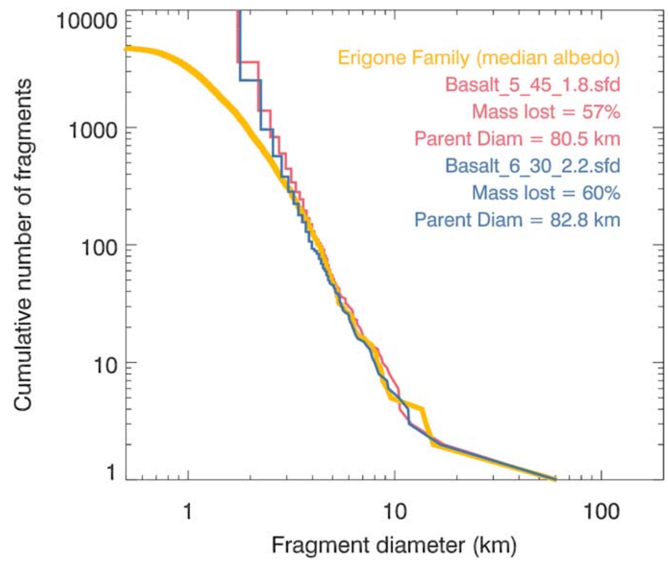

Figure 8. Two modeled fragment SFDs compared to the observed Erigone family SFD. The latter is the gold curve, and it comes from Figure 4. The modeled fragment SFDs come from D. D. Durda et al. (2007). For the red curve, defined as "Basalt_5_45_1.8," a 100 km diameter solid basalt target was hit at 5 km s^{-1} at a 45° impact angle, with the logarithm of the target-to-projectile mass ratio being 1.8 (i.e., a 25 km diameter projectile). For the blue curve "Basalt_6_30_2.2," a 100 km diameter target was hit at 6 km s^{-1} at a 30° impact angle by an 18 km diameter projectile. The fragment SFDs from both runs were scaled to fit the observed Erigone family SFD. For the red curve the net mass in the fragment SFD, excluding the largest remnant, is 57% of the parent body, which we estimate was 80.5 km in diameter, while for the blue curve the values are 60% and 82.5 km, respectively.

logarithm of the target-to-projectile mass ratio (see D. D. Durda et al. 2007, for details). Thus, for example, model Basalt_5_45_1.8 involved a 100 km diameter solid basalt target, impacted at 5 km s^{-1} at a 45° impact angle by a 25 km diameter projectile.

Overall, the fit between the two models is reasonable. We find that the red curve (Basalt_5_45_1.8) provides a marginally better fit than the blue curve (Basalt_6_30_2.2) because the red curve stays near or above the observed SFD. With that said, some of this is in the eye of the beholder; neither the red nor the blue curve fit the gold curve near $D = 15$ km. This mismatch could stem from interlopers, collisional evolution in the family over its lifetime, a poor estimate of the diameters of these bodies, the use of basalt rather than carbonaceous-chondrite-like material, and so on. A closer inspection of the large members of the Erigone family does indicate that the reported error on their albedos is compatible with that of Erigone. We note, however, that these objects could be elongated, in which case the reported diameter would be biased toward larger size depending on observational geometry. The reader should also keep in mind that the SPH runs have a resolution limit, so all of the mass has to go somewhere, usually into the smallest particles. This behavior explains why the SPH SFDs become steep for $D < 2$ km.

Both model fits suggest that the Erigone parent body size was close to 80 km in diameter. Calculating the mass remaining in the model fragment SFDs and comparing that to the model parent body sizes, we predict that the Erigone family was produced by an impact modestly larger than a barely catastrophic disruption, where "catastrophic" means that >50% of the mass was ejected away at escape velocity. Both simulations show that roughly 60% of the mass was put into family fragments. This would rule out the hypothesis that the Erigone family was created in a large cratering event.

These values should be considered preliminary estimates for the properties of the Erigone-family-forming event. Given the current inability of the D. D. Durda et al. (2007) model to match the SFD from WISE observations, additional work will be needed to see whether this is a by-product of an inadequate model or an interpretation issue affecting the observational data.

Collisional age of the Erigone family. Immediately after the Erigone family was created, the family members began to be hit by asteroids from the background main-belt population, which is nearly 3 orders of magnitude larger than the Erigone family itself (i.e., one can compare the Erigone family SFD in Figure 4 to the main-belt SFDs shown in Figure 1 of W. F. Bottke et al. 2020). Over time, these impacts will break down the Erigone family SFD, such that it will take on the same shape as the main-belt SFD (e.g., W. F. Bottke et al. 2005a, 2007, 2015a; M. Brož et al. 2024b, 2024a). Ideally, the shape change can be used like a clock to determine the age of the Erigone family, provided that it is old enough that its observed SFD has had sufficient time to be noticeably affected by collisional evolution. The diagnostic constraint would be to find a portion of the family SFD with a shape that is congruent with that of the main-belt SFD.

We decided to investigate this issue using the Collisional and Dynamical Depletion Evolution Model (CoDDEM) described in W. F. Bottke et al. (2005a, 2005b). This code was used to track the collisional evolution of the main-belt SFD over its history. Within this 1D code, W. F. Bottke et al. (2005a, 2005b) simulated how impacts changed the number of objects in a set of diameter bins (i.e., lower limit D, upper limit $D + dD$) between $0.0001\ \mathrm{km} < D < 1000\ \mathrm{km}$, with logarithmic intervals set to $d \log D = 0.1$. Starting assumptions and computational details are provided in those papers.

The most recent CoDDEM formulation of the main-belt SFD can be found in W. F. Bottke et al. (2020). They used it to model crater SFDs on spacecraft-observed asteroids like Ceres, Vesta, Lutetia, Mathilde, Ida, Gaspra, and Eros, all which have $D > 10$ km. Their crater SFDs have wavy shapes and spanned sizes between 0.1 and 100 km. Assuming that the crater-to-projectile ratio is $\approx$10, as argued in W. F. Bottke et al. (2020), these sizes correspond to asteroid diameters between 0.01 and 10 km (see below for more details about crater scaling laws). Accordingly, these data make it possible to constrain the shape of the main-belt SFD well below the observational limit. Given that their preferred model main-belt SFD provided an excellent match to these crater SFDs, one can make a case that the CoDDEM model and results from W. F. Bottke et al. (2020) can be used to simulate the collisional evolution of the Erigone family to reasonable approximation. This will be accomplished by (i) inserting an estimate of the initial Erigone family SFD into CoDDEM, (ii) tracking what happens to it over different family ages (T), and (iii) comparing the results to the observed Erigone family SFD.

Our choice for the observed Erigone family SFD will come from Figure 4. We will use the red curve, namely the SFD constructed using the absolute magnitudes and the median albedo of Erigone family members. The shape of the initial family SFD was determined through the following process: First, we tested how the observed SFD experienced collisional evolution over a range of T values between 100 and 500 Myr.

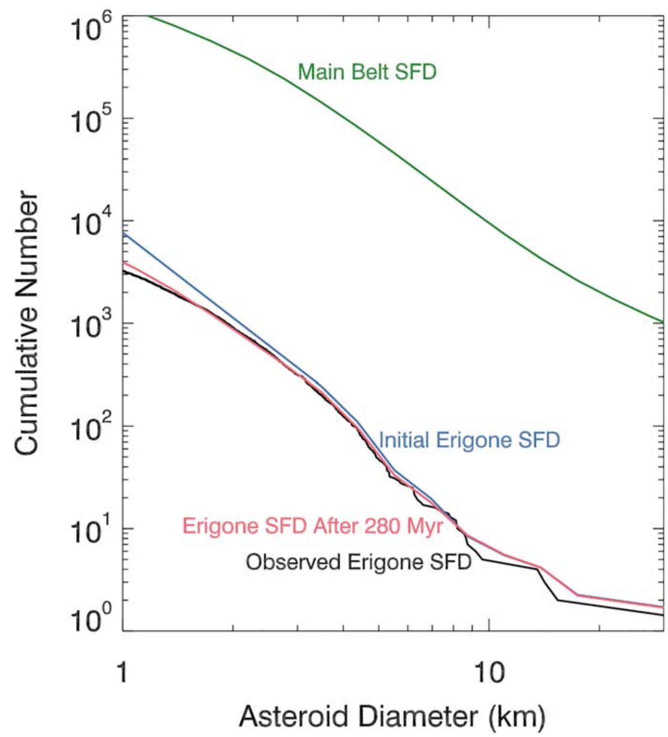

Figure 9. Collisional evolution of the Erigone family SFD. The green curve represents the main-belt SFD as formulated by W. F. Bottke et al. (2020). The blue curve is our estimate of the initial Erigone family SFD. The black curve is the observed Erigone family SFD determined using absolute magnitudes and the family's median albedo (red curve in Figure 4). The red curve shows the Erigone family SFD after 280 Myr of collisional evolution.

We found that most collisions mainly affected the number of $D < 8$ km asteroids in the family SFD by a factor f but only modestly affected the overall shape of the SFD. This meant that we could multiply the $D < 8$ km objects by f and more or less reproduce the observed Erigone family SFD in time T.

Second, we extrapolated the observed cumulative Erigone family SFD between $2\ \mathrm{km} < D < 4$ km to smaller fragment sizes with $D < 2$ km. The cumulative power-law slope found for this extrapolation was $q = -2.76$. For this preliminary exercise, we avoid using the hydrocode models from the previous section, mainly because resolution issues mean that the smaller sizes in the fragment SFD have more mass than they should in reality. We should also state as a caveat that we do not know whether our assumption of a power-law SFD for $D < 4$ km is valid, only that we do not have a better approximation.

Finally, we used both components to test various T values, with the goal being to reproduce the observed SFD for $D < 2$ km. After some trial and error, we found the results that are shown in Figure 9. The green curve is the cumulative main-belt SFD from W. F. Bottke et al. (2020; their main-belt formulation 6), the black curve is the observed cumulative SFD, the blue curve is our estimate of the initial Erigone family SFD with $f = 1.2$, and the red curve is what the model SFD looks like after 280 Myr. Overall, the shape of the observed SFD is reproduced. There is a small mismatch near $D \approx 1$ km, but we suspect that this is from observational incompleteness in the observed Erigone family.

The reader should consider these results to be preliminary and approximate. We believe they should be revisited after Lucy's encounter with DJ, when we will know more about the physical properties of a real Erigone family member. With that said, these results help substantiate the dynamical ages suggested earlier in the text, namely that the Erigone asteroid family is $T < 300$ Myr old. Finally, we note that a typical 4 km main-belt asteroid has a collisional lifetime exceeding 1 Gyr (Figure 1 in S. Marchi et al. 2006); thus, it is likely that DJ has retained the overall bulk properties since its formation.

2.2. Does DJ Belong to the Erigone Family?

At this time, DJ's membership in the Erigone family is mainly based on circumstantial evidence. Given the available information, we believe that the pros outweigh the cons. We list some of our arguments below.

First, the number of interlopers in the Erigone family has been found to be low, especially for $a_P > a_c$ away from the z_2 secular resonance. DJ's $a_P \simeq 2.384$ au meets this condition and avoids interaction with any meaningfully strong mean motion resonance.

As for DJ's orbital location, we note its high $e_P \simeq 0.214$ value, which helps to explain its short orbital Lyapunov timescale of $\simeq$12 kyr. Tracking its orbits forward for 10 Myr, we find that DJ's perihelion distance may reach $\simeq$1.727 au. While this is not close enough to have a close encounter with Mars, it can approach this planet within several tens of its Hill radius. This leads to weak chaotic behavior in its orbit, a phenomenon termed "stable chaos" by A. Milani & A. M. Nobili (1992).

This result prompted us to test what would happen to DJ over longer timescales. Here we used `swift`, a well-tested numerical package dedicated to integration of the $(N + M)$-body problem (the Sun and $N - 1$ massive planets plus M massless particles), to propagate DJ's nominal orbit and 50 close clones forward in time for 1 Gyr. We included all eight planets and used a short time step of 3 days. We output our results every 5 kyr. We found that none of our DJ test asteroids were eliminated over the 1 Gyr time span. The instability timescale in DJ's orbital zone is therefore comfortably longer than the estimated age of the Erigone family.

We also found that the proper value of the semimajor axis a_P of the clones experienced a random walk. In 200 Myr, their values were distributed in the interval $(-1, +2) \times 10^{-3}$ au about the initial value. This range is about an order of magnitude smaller than the expected semimajor axis changes caused by the Yarkovsky effect (see Figure 13 for a rough estimate of the Yarkovsky shift of DJ over the best-fit Erigone family age of 155 Myr). It is therefore unlikely that large asteroids from the Erigone zone where DJ is located have leaked into the terrestrial planet region.

Note that the situation may be different for Erigone members having similar e_P values to DJ but $a_P \leqslant 2.35$ au (see the top left panel of Figure 2). Here the bodies may be assisted by some weak mean motion resonances such as (J9,-S6,-2) at $a_P \simeq 2.35$ au or J10/3 at $a_P \simeq 2.33$ au.

Second, the prograde rotation and small obliquity value for DJ appear consistent with expectations based on our Yarkovsky/YORP evolution model (see also Appendix A.3 for context). DJ's $a_P \simeq 2.384$ au represents the transverse velocity difference of nearly 60 m s^{-1} with respect to the family center a_c. Our typical Yarkovsky/YORP evolution solutions presented in Section 2.1 resulted in $v_5 \simeq 20$ m s^{-1}. This means that it is unlikely that DJ was initially ejected to its current orbital location. Rather, at least half of its semimajor axis distance from the family center was acquired by past Yarkovsky evolution. For that assertion to be true, DJ's past drift rate in a_P must have been positive, which requires prograde rotation. The independent determination of its rotation pole by recent telescopic observations (S. Mottola 2024, personal communication) is therefore supportive of this model. DJ's slow rotation rate implies only a small lag between heating its surface by sunlight and thermal reemission. As a consequence, the Yarkovsky effect is not optimum for its size. Indeed, DJ's location in the (a_P, H) plane (bottom left panel of Figure 2) stays away from the "wave front" at the $C_\star$ isoline. Given our best-guess parameters for DJ, we estimate a semimajor axis drift rate to be $da/dt \simeq 8.4 \times 10^{-5}$ au Myr^{-1}. Thus, the timescale to drift from the center of the family at a_c is about 172 Myr (see Figure 13 for more details).

Third, we consider DJ's slow rotation rate. The question is whether DJ's current rotation period of $P \simeq 252$ hr is compatible with an initial value of $P_0 \leqslant 24$ hr followed by YORP evolution over a time interval constrained by the Erigone family age. We do not have the YORP effect measured for this asteroid, but we take the value detected for (1620) Geographos as a plausible template. Like DJ, Geographos is a very elongated object with a similar obliquity value and YORP rotation rate acceleration $d\omega/dt = (1.14 \pm 0.03) \times 10^{-8}$ rad day^{-2} (e.g., J. Ďurech et al 2022).

Considering that the strength of YORP scales with size D, semimajor axis a, and bulk density ρ, $d\omega/dt \propto \rho^{-1}(Da)^{-2}$, we obtain an estimate $d\omega/dt \simeq 2 \times 10^{-9}$ rad day^{-2} for DJ (for simplicity, we take 10^{-9} rad day^{-2}). Note that Geographos's rotation rate is accelerating by YORP, while here we assume that the opposite evolution took place for DJ. Assuming that YORP has been decelerating DJ's rotation at the constant rate estimated above, and denoting $\kappa = 2\pi/P/(d\omega/dt) \simeq 1.64$ Myr, we estimate the required time T to reach the current rotation period P from its initial value P_0 as $T \simeq \kappa\ (P/P_0 - 1)$. Taking $P_0 \simeq 6$ hr, we get $T \simeq 70$ Myr. This value is shorter than the estimated age of the Erigone family, making it plausible that DJ formed from the Erigone-family-forming event.

Similarly, the YORP torque is able to change DJ's obliquity from a generic prograde initial state to near zero value on a timescale of approximately equal to the above-estimated T for rotation rate evolution.[5]

An alternative possibility to the evolution of the rotation state by the YORP torques described above is that of a minimum amount of evolution. In that case, the current rotation would reflect the initial state at the Erigone family formation. Consider, for instance, that the DJ rotation is in fact in a tumbling state that would not be that surprising given its slow rotation (see, e.g., Figure 8 in P. Pravec et al. 2014, which indicates that DJ is in the midst of parameter space populated by detected tumblers). The uncertainty of the corresponding damping timescale is dominated by the unknown internal dissipation rate parameters, namely a product of the elasticity modulus μ and quality factor Q. But even in an optimistic situation $\mu Q \simeq 10^9$ Pa, DJ's tumbling requires more than a

[5] Equations (3) and (5) in D. Čapek & D. Vokrouhlický (2004), together with a characteristic YORP torque $T_\epsilon/C \propto -\sin\epsilon$ for prograde obliquities ϵ, provide an approximate solution $\tan[\epsilon(t)/2] = \tan(\epsilon_0/2)\,(1 - t/T)^\alpha$ with the initial value ϵ_0, the timescale $T = \omega_0/(d\omega/dt)$ as in the main text, and the power exponent $\alpha = T\,(d\epsilon/dt)_0$ (ω_0 is the initial rotation rate and $(d\epsilon/dt)_0$ the maximum obliquity rate for an asteroid rotation at frequency ω_0). From data in Section 4 of D. Čapek & D. Vokrouhlický (2004) we estimate $(d\epsilon/dt)_0 \simeq 1°$ Myr^{-1} and thus $\alpha \simeq 1.2$.

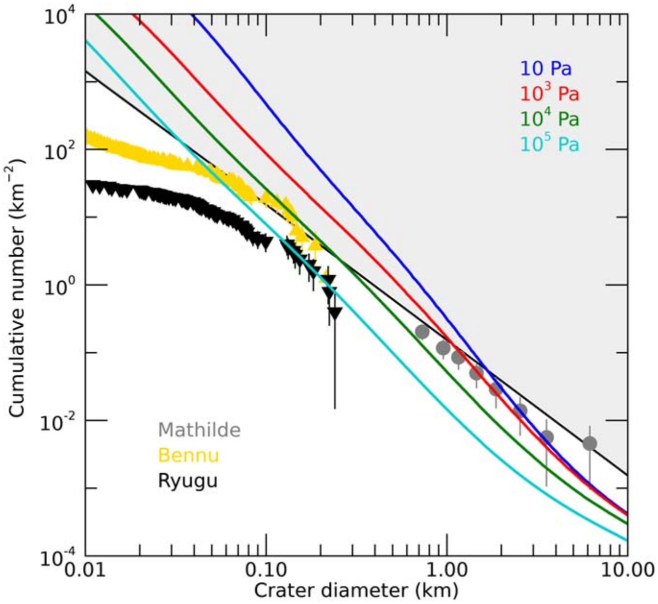

Figure 10. Solid curves indicate our model crater SFDs for various target strength values Y (as shown by the labels). The black line corresponds to the empirical crater surface saturation, as 10% of the geometric saturation (S. Marchi et al. 2015). Observed crater SFDs for Bennu, Ryugu, and Mathilde are given for sake of comparison (yellow, green, and gray, respectively; data from C. R. Chapman et al. 1999; W. F. Bottke et al. 2020).

100 Myr timescale to become damped (see Section 5.1 of P. Pravec et al. 2014). Note also that the tumbling rotation state of DJ would not conflict with its semimajor axis secular drift by the Yarkovsky effect. This is because the Yarkovsky effect has been both predicted and detected for a number of tumbling near-Earth asteroids, including (99942) Apophis and (4179) Toutatis (e.g., D. Vokrouhlický et al. 2015; D. Farnocchia et al. 2024).

3. Implications for Lucy Mission Flyby

Here we explore the collisional history of DJ and make predictions on its surface crater SFD. These studies will serve as a reference and will support further analyses of the Lucy mission data.

For craters on DJ, we used the Pi-group scaling law (e.g., K. A. Holsapple & K. R. Housen 2007a, 2007b) that provides the transient crater diameter as a function of impact conditions and material properties. We further assume the final crater to be ∼30% larger than the transient crater (e.g., S. Marchi et al. 2015, 2023).

We calculated median values of the intrinsic collision probability P_i and impact velocity V_i using a sample of main-belt asteroids larger than 50 km (P. Farinella & D. R. Davis 1992) and obtained $P_i = 3.94 \times 10^{-18}$ km^{-2} yr^{-1} and $V_i = 5.14$ km s^{-1}. Figure 10 shows the computed crater cumulative SFD for DJ assuming a 150 Myr surface age corresponding to the best-fit family age. We implemented a cohesive soil cratering scaling law with various values of target strength (Y), namely $Y = 10$, 10^3, 10^4, and 10^5 Pa.

We stress that the strength of the target material is not known, and our assumptions provide a reasonable range of properties. For instance, M. E. Perry et al. (2022) found that the Bennu surface strength is less than 2 Pa, based on the ejecta pattern of a 70 m diameter crater. On the other hand, R. L. Ballouz et al. (2020) concluded that meter-sized boulders on Bennu have a strength of 0.5−1.7 MPa. These strength values, however, are inferred from meter-scale properties, and their applicability to larger craters on DJ is not clear.

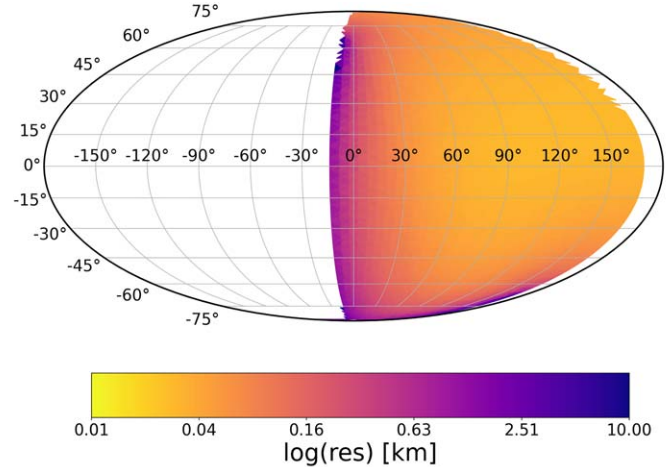

Figure 11. Expected DJ surface coverage from the Lucy flyby. The best resolution is about 10 m pixel^{-1} (H. A. Weaver et al. 2023; the term "res" indicates a resolution element and corresponds to 3 L'LORRI pixels). Craters as small as 100 m in diameter could be resolved on about one-third of the imaged surface. However, we stress that this image assumes a spherical target, which may not be realistic.

Our calculations show an interesting result, namely the crater SFD in the size range observable by Lucy (>100 m in diameter) is sensitive to the material strength, with shallower slopes for increased strength Y in the range $10-10^5$ Pa. When compared to a simple model for crater surface saturation (e.g., S. Marchi et al. 2015), we find that DJ craters smaller than 1−2 km could be saturated even for the assumed young surface age for terrain strength $Y < 10^4$ Pa. For higher Y values, the computed crater SFD drops below saturation. Figure 10 also shows the crater SFDs of Bennu, Ryugu, and Mathilde (all C types) for comparison. Note that Bennu (≃0.49 km size) and Ryugu (∼0.90 km size) are significantly smaller than DJ, while Mathilde (∼53 km size) is significantly larger than DJ. Therefore, DJ fills a gap of asteroid size concerning crater SFDs previously explored and measured by spacecraft.

The Lucy mission will fly by DJ and observe its surface with the high-resolution L'LORRI imager (H. A. Weaver et al. 2023). These observations are, however, limited by the fact that all observations will terminate ∼40 s before the closest-approach distance owing to solar elongation avoidance constraints. As a result, only 50% of DJ's surface will be imaged. The anticipated coverage and spatial resolution are shown in Figure 11. It is expected that Lucy will provide data in a crater size range between 100 m and a few kilometers (depending on DJ's actual size), which is a size range not covered by Bennu/Ryugu and Mathilde.

4. Conclusions

In this paper, we presented our current understanding of the formation and evolution of the Erigone asteroid family and its member DJ, a flyby target of the NASA Lucy mission (slated for 2025 April 20). Due to a richness of available data regarding Erigone's family members, Erigone is an exemplary family for detailed studies of collisional formation and evolution. We show that the Erigone family is young (<250 Myr), and its fine orbital structure allows us to quantitatively constrain the physical parameters of DJ (e.g., density, thermal inertia).

The intention of this paper is to push the predicting potential of our dynamical and collisional models to the best of our capabilities and then use Lucy flyby data to test our predictions. Given DJ's inferred shape, spin state, composition, and collisional evolution, the DJ flyby offers a unique opportunity to test a wide range of model predictions.

In addition, the Erigone family is close to a cluster of primitive families in the inner main belt, where Bennu and Ryugu originated. This offers a unique opportunity to study at close range a larger sibling in the native main-belt environment before being pushed to near-Earth space or being shattered to smaller fragments by a catastrophic collision.

Finally, a note on the broader interest of the DJ flyby. The Lucy science team named asteroid DJ in honor of the discoverer of the 3.2 million year old Lucy hominin (and namesake for the Lucy mission), paleoantropologist Donald Johanson. As such, this is the first case in the history of space exploration in which a spacecraft visits an asteroid named after a contemporary human.

Acknowledgments

S.M., W.F.B., and H.F.L. acknowledge support from the Lucy mission, financed through the NASA Discovery program through contract No. NNM16AA08C. We thank M. Brož for providing us with a compilation of WISE albedo data. The work of D.V. and J.D. was partially supported by the Czech Science Foundation (grant 23-04946S).

Appendix
More Details about the Erigone Family

A.1. Determination of the Formal Family Center and Critical Borderline in C Parameter

In order to make selection of the exterior interloper region in the (a_P, H) plane objective (Figure 2), we recall definition of the C parameter using Equation (1). The sought family limit is one of the C-isolines with a fine-tuned value $C_\star$. The method of finding $C_\star$, as well as the formal family center a_c, was originally proposed by K. J. Walsh et al. (2013) and further developed by B. T. Bolin et al. (2017, 2018).

Since most of the asteroid families—including Erigone—do not exhibit huge asymmetries in distribution of their members in the (a_P, H) plane (unless located close to major mean motion resonances), a_c is typically located very near the largest asteroid in the family (in our case this would be at the proper semimajor axis of (163) Erigone). However, to cope with a slight degree of asymmetry, we rather adjust a_c in order to match distribution of the bulk of smaller members in the family. The method proceeds as follows: Assume that C_1 and C_2 are two equal-sign values of the C parameter defined in Equation (1) and $|C_2| > |C_1|$. Let then $N(C_1, C_2; a_c)$ denote the number of asteroids in between these two isolines. We use N in two neighbor zones of width ΔC (in practice, we implemented $\Delta C = 3 \times 10^{-6}$ au) adjacent to a C-isoline to seek the largest drop in the population (see the bottom left panel of Figure 2 to note the zones up to which Erigone members piled up by the Yarkovsky drift). To determine the population contrast of the two neighbor intervals to C, we thus define

$$r_+(C, a_c; \Delta C) = \frac{N(C - \Delta C, C; a_c)}{N(C, C + \Delta C; a_c)} \tag{A1}$$

for C positive and

$$r_-(C, a_c; \Delta C) = \frac{N(C + \Delta C, C; a_c)}{N(C, C - \Delta C; a_c)} \tag{A2}$$

for C negative. As we do not expect a significant asymmetry in Erigone member distribution in the (a_P, H) plane, we define the total contrast function

$$r(C, a_c; \Delta C) = r_+(C, a_c; \Delta C)\, r_-(-C, a_c; \Delta C) \tag{A3}$$

for C positive. We now seek optimum values of a_c and $C_\star = C$ to maximize $r(C, a_c; \Delta C)$. Searching $a_c \in (2.366, 2.374)$ au and $C \in (1.2, 2.0) \times 10^{-5}$ au, we found the best solution $a_c = 2.3695$ au and $C_\star = 1.7 \times 10^{-5}$ au. These are the parameters used in the bottom left panel of Figure 2 (vertical dashed line and solid gray C-isolines).

A.2. Erigone Population Completeness at H = 17.5 mag Limit

We used observations by Catalina Sky Survey (CSS), Mt. Lemmon survey telescope (IAU code G96), in between 2013 January and 2023 July. D. Nesvorný et al. (2024b) performed a detailed analysis of the detection efficiency of hundreds of thousands of fields of view taken by the telescope during this period of time, helping them to develop a new population model for the near-Earth asteroid population. Here we use the same database of well-calibrated observations with known sky coverage to infer detection probability of orbits in the Erigone family zone.

First, we simply sifted all the CSS/G96 frames taken in the 2013–2023 decade and searched for detections of the members in our nominal Erigone family (Section 2.1). Out of all 4925 members, CSS observed 4291 of them, missing just 634 asteroids. In the group of unobserved members, only (20992) Marypearse stands out with its $H = 15.52$ mag. All others, starting with (391495) 2007 OV10, have $H \geqslant 17.62$ and are thus small members (some of which have been even discovered after 2023 July). In fact, only three of them have the absolute magnitude $H < 18$ (all of them having $a_P > 2.38$ au).

Second, we created two samples of 15,000 synthetic orbits in the Erigone family by considering their real orbits with semimajor axes in the ranges (2.32, 2.33) au (first sample) and (2.41, 2.43) au. We assigned them their osculating orbital elements as of the MJD 60600.0 epoch, with the only exception of the mean anomaly that was randomized in the 0°–360° range. These orbits were propagated backward in time to 2013 January with the goal of inferring whether (i) they would fall in one of the CSS fields of view and (ii) if so, whether the telescope would detect them. To that end, we use the publicly available and well-tested `objectsInField` code from the Asteroid Survey Simulator package (S. P. Naidu et al. 2017). We found that in the first sample all objects with $H \leqslant 17.3$ have basically 100% detection probability and those with $H = 17.5$ have 99.2% detection probability. Likewise, objects in the second sample have 100% detection probability for $H \leqslant 17.05$ mag, and even those with $H = 17.5$ have 97.5% detection probability. Beyond magnitude $H = 18$ the detection probability drops below 90%, and there is approximately 0.25 mag shift in between the two samples to reach the same

Table 1
Erigone Family Members with Known Rotation Models

Number	Designation	P (hr)	$(\lambda, \beta)_1$ (deg)	$(\lambda, \beta)_2$ (deg)	(ϵ_1, ϵ_2) (deg)	D (km)	p_V	Taxonomy	References
163	Erigone	16.14	(303, −67)	⋯	(160,−)	69.4	0.027	Ch,T	(3, 4, 5)
933	Susi	4.62	(299, −13)	(122, −15)	(105, 103)	24.7	0.027	T	(3, 4)
1448	Lindbladia	10.97	(83, 49)	(273, 38)	(45, 48)	22.7	0.025	⋯	(3)
2776	Baikal	3252.41	(90, −39)	(270, −27)	(124, 122)	18.3	0.033	Cgh	(3, 5)
5026	Martes	4.42	(199, 51)	(14, 60)	(35, 34)	9.0	0.066	Ch	(1, 2, 3)
5506	Artiglio	9.41	(50, 78)	(245, 69)	(15, 18)	13.1	0.039	X	(3, 5)
8612	Burov	6.14	(225, −20)	(49, −10)	(106, 104)	5.2	0.079	⋯	(5)
9566	Rykhlova	8.57	(151, −72)	(328, −73)	(159, 167)	9.3	0.065	Ch	(3, 4)
10527	1990 UN1	5.78	(51, −73)	(240, −60)	(158, 155)	8.1	0.050	⋯	(3)
14355	1987 SL5	6.63	(260, 62)	(94, 58)	(31, 29)	6.9	0.057	⋯	(3)
15758	1992 FT1	7.55	(77, 45)	(259, 33)	(50, 52)	9.4	0.038	⋯	(3)
18595	1998 BR1	6.02	(158, −75)	⋯	(170,−)	11.5	0.053	⋯	(3)
18851	Winmesser	27.32	(302, 24)	(125, 19)	(68, 69)	7.6	0.058	⋯	(3)
24723	1991 TW8	6.17	(32, 29)	(220, 27)	(62, 61)	4.2	⋯	⋯	⋯
24837	Msecke Zehrovice	155.76	(13, −66)	(232, −72)	(157, 163)	5.3	⋯	⋯	⋯
30772	1986 RJ1	8.06	(80, 55)	(259, 41)	(40, 44)	6.3	0.092	⋯	(3)
41707	2000 UU55	13.35	(6, −58)	(185, −42)	(142, 138)	5.7	0.072	⋯	(3)
44942	1999 VM55	4.56	(107, 32)	(284, 42)	(54, 52)	5.0	0.060	X	(3, 4)
49859	1999 XB100	12.58	(29, −50)	(211, −57)	(144, 164)	7.4	0.055	Cgh	(3, 4, 5)
55440	2001 TY85	428.09	(53, −72)	(234, −77)	(165, 164)	4.9	0.072	⋯	(3)
61815	2000 QZ189	9.21	(199, −21)	(20, −34)	(117, 118)	5.2	0.059	⋯	(3)
64771	2001 XM180	22.25	(179, −40)	(345, −48)	(134, 135)	6.5	0.038	⋯	(3)
66325	1999 JF55	13.91	(136, −54)	(292, −59)	(148, 146)	5.6	0.088	Xc	(3, 4)
91345	1999 JK36	369.06	(327, 60)	(127, 81)	(25, 14)	5.6	0.055	⋯	(3)
98345	2000 SQ304	8.02	(95, −65)	(292, −70)	(157, 159)	4.6	0.063	Cg	(3, 4)
153364	2001 QL	6.80	(196, −67)	(37, −63)	(155, 156)	4.8	0.059	⋯	(3)

Note. The third column provides the sidereal rotation period P, the fourth and fifth columns provide the ecliptic longitude λ and latitude β of the rotation pole (photometric data analysis of the main-belt asteroids often results in $\sim180^\circ$ degeneracy of λ, hence the two pole solutions in some cases), the sixth column provides obliquity ϵ of the pole solution(s), the seventh and eight columns give size D and geometric albedo p_V from WISE data (except in cases not observed by WISE for which the size is estimated from the absolute magnitude value and albedo $\bar{p}_V = 0.057$), the ninth column gives the spectral class, and the 10th column provides principal references: (1) P. Pravec et al. (2019); (2) D. Polishook et al. (2014); (3) J. R. Masiero et al. (2011); (4) D. Morate et al. (2016); (5) B. Harvison et al. (2024). The associated shape models, when available, and other information could be downloaded from the DAMIT website (see also J. Ďurech et al. 2010).

detection probability (i.e., in the group with smaller semimajor axes objects with absolute magnitude larger by about 0.25 are detected with the same probability as those in the group with larger semimajor axes). This bias is seen in the bottom left panel of Figure 2.

From this exercise, taking into account only CSS observations, we infer near completeness of the Erigone family at $H = 17.5$ mag. This conclusion would even be strengthened if well-characterized observations by other prolific surveys (Sun as Pan-STARRS) were available to us. The result also agrees with that reached by an independent method in N. P. Hendler & R. Malhotra (2020).

A.3. Erigone Members with Known Rotation State

The Yarkovsky/YORP evolution model of the families, when applicable, implies a particular distribution of rotation state of their members. This is because Yarkovsky-driven migration to large or small values of the proper semimajor axis a_P requires prograde or retrograde rotation state. The analysis of sparse photometry, provided by powerful ground- and space-based surveys, recently allowed us to significantly increase the sample of asteroids with resolved rotation state. Consequently, the Yarkovsky/YORP dynamical models for a number of asteroid families could have been eventually tested (see J. Ďurech & J. Hanuš 2023, for several spectacular examples).

While solutions for spin state of several Erigone members have been previously published, we decided to reevaluate them with a critical eye on statistically borderline cases. To that goal, we collected sparse photometry from the main sky surveys (for details, see J. Hanuš et al. 2023) of Erigone members and used the lightcurve inversion method of M. Kaasalainen et al. (2001). In some cases we found previously published models to be not statistically robust enough, and in several other cases we obtained new solutions. The final models are summarized in Table 1. We note that the available photometric data allow us to solve for rotation period and pole of five more nominal members in the Erigone family, namely (12642) Davidjansen, (62040) 2000 RA64, (66309) 1999 JX41, (66403) 1999 LM3, and (229334) 2005 QV4. However, analysis of their color indices (see Figure 12) suggests that they belong to the high-albedo interloper class; consequently, we discarded them from the valid sample of Erigone asteroids with resolved spin state.[6] As shown by J. Ďurech et al. (2020), the slope of the phase curve (defined as the ratio of the theoretical phase curve function at 10° and 20° of the solar phase angle) and the color index c–o in ATLAS c and o filters are correlated with albedo—low-albedo C-complex asteroids have higher slope and smaller difference between c and o filters, while

[6] In the case of (12642) Davidjansen and (66309) 1999 JX41 this conclusion is also supported by broadband photometry data from SDSS, since their principal component value $a^\star > 0.1$ makes them belong to the high-albedo S-type taxonomic group (e.g., A. Parker et al. 2008).

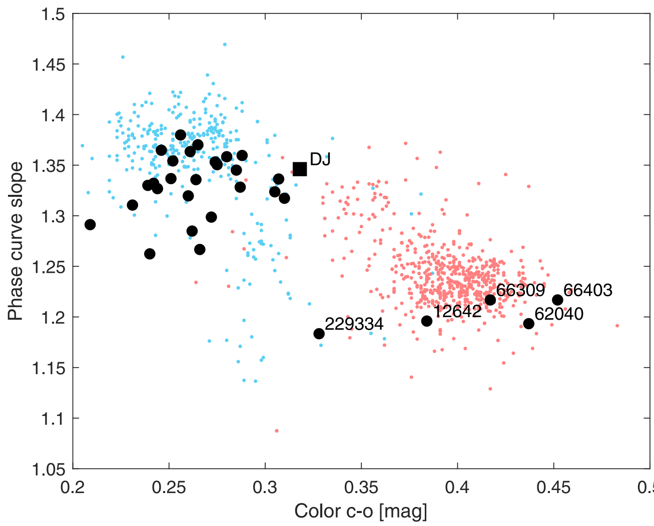

Figure 12. Color index *c–o* defined as a difference between magnitudes in cyan and orange ATLAS filters (abscissa) and slope of the phase curve (ordinate) for asteroids (i) that are nominally members of the Erigone family and (ii) for which the available photometric data allow us to determine their rotation state (i.e., sidereal rotation period and pole orientation). The distinct cluster of black points characterized by a small color index and large slope corresponds to Erigone family members with low albedo (these are listed in Table 1). Importantly, DJ—shown as a black square—appears to belong to this group. Additionally, there are five asteroids, identified by their numbers, clearly separated from the main cluster by having larger color index and smaller slope values. These are likely interlopers with high albedo and affinity to S-taxonomic class. As a result, we disregard them in our further analysis. The underlying red and blue points are known asteroids of S and C taxonomic class, respectively, projected onto these axes (compare with Figure 4 in J. Ďurech et al. 2020).

high-albedo S-complex asteroids have smaller slope and larger difference between filters. Because all modeled Erigone family members have observations from the ATLAS telescopes in both filters,[7] we can use this diagnosis tool for detecting high-albedo interlopers (Figure 12).

Figure 13 (left panel) displays the results in the relevant projection to the plane of proper semimajor axis a_P and absolute magnitude H. As outlined above, we expect prograde-rotating members (red symbols) to be located in the $a_P > a_c$ zone and retrograde-rotating members (blue symbols) to be located in the $a_P < a_c$ zone. The largest members, or those with the rotation pole near enough to the ecliptic plane, may be located near the family center. In order to characterize what "the center" means for asteroids of a different magnitude value, we consider the formally best-fit Yarkovsky/YORP model from Section 2.1 that had $v_5 = 24\,\mathrm{m\,s^{-1}}$ initial ejection velocity of $D = 5\,\mathrm{km}$ fragments (and $v_{\mathrm{ej}} \propto 1/D$ for other fragments). Their initial location is highlighted by the light-gray region near the family center (assuming the isotropic ejection field of the fragments). Finally, we consider the estimated value of the Yarkovsky drift da_P/dt using the present-day obliquity and parameters of the best-fit model, in particular the 155 Myr age of the Erigone family, and mapped the current to the initial asteroid location (see the color intervals). This procedure is obviously highly simplified, as no YORP modification of the rotation parameters is taken into account, but provides at least a zero-order estimate of the asteroid evolution in these coordinates over the predicted family age. The right panel of Figure 13 shows the distribution of rotation rate values for Erigone fragments: the distribution for the most complete models, for which also the rotation pole has been determined (Table 1), is highlighted in red, while the gray histogram is for all Erigone members (period solutions for cases in which the rotation pole has not been determined were taken from the LCDB database; see B. D. Warner et al. 2009). In either case, the rotation rate distribution cannot be matched with a Maxwellian model for the collisionally relaxed population. The surplus of slowly rotating objects hints at traces of a population evolved by the YORP effect (see P. Pravec et al. 2008, for context).

Overall the limited data provide an excellent justification of the model, since (i) the prograde- and retrograde-rotating members are all located in their respective zones; (ii) the estimated evolutionary tracks connect their position to the zone, where they should be located initially; and (iii) the rotation rate distribution reveals perturbation by the YORP effect. We expect that this picture will be even strengthened when more solutions are added in the future.

A.4. Outline of the Yarkovsky/YORP Chronology Approach

The method of Yarkovsky/YORP chronology of the asteroid families has been developed in D. Vokrouhlický et al. (2006b), with a precursor version dwelling on the Yarkovsky component in D. Nesvorný et al. (2003). Since both D. Vokrouhlický et al. (2006b) and W. F. Bottke et al. (2015b) provide a detailed description of the approach, here we list the principal steps in brief (relegating the reader to those references for more information if needed).

We assume that the family has been represented using the differential distribution $dN(C)$ with the C parameter defined by Equation (1). In the case of the Erigone family, we determined the family center a_c and maximum-contrast $C_\star$ parameter in Appendix A.1. In order to describe the drop in the family population beyond $C_\star$, we extend $dN(C)$ to $C_{\mathrm{fam}} = 1.95 \times 10^{-5}$ au, at which the family population is effectively nil. We use the finite bin size $\Delta C = 1.5 \times 10^{-6}$ au to represent the distribution, and we use the symmetric version $dN_{\mathrm{sym}}(C)$ defined in Equation (2). In order to minimize contamination by interlopers and avoid problems with uncertain modeling of the YORP evolution over several of its cycles (evolution from generic initial conditions to the asymptotic state), we used 640 Erigone dark members with $H \leqslant 17.5$ to construct these data.

The goal of the model is to match the observed-family $dN_{\mathrm{sym}}(C)$ distribution with prediction $dM(C; \boldsymbol{p})$ by minimization of target function (3). The minimization is achieved by determining the optimum (best-fit) model parameters $\boldsymbol{p}$. We split $\boldsymbol{p}$ into two categories: (i) the original set introduced by D. Vokrouhlický et al. (2006b), and (ii) additional parameters adopted by D. Vokrouhlický et al. (2006b), but given that their uncertainty also appreciably affects the results, we decided to include them in the present work. The first set consists of (i) the family age T, (ii) the characteristic initial ejection velocity v_5 of 5 km size fragments (fragments of size D are assumed to be ejected with velocity v_5 (5 km/D)), and (iii) the empirical YORP torque strength parameter c_{YORP}, adjusting them against a simple template taken from D. Čapek & D. Vokrouhlický (2004). The second set includes (i) asteroids' bulk density ρ, (ii) asteroids' surface thermal inertia Γ, and (iii) characteristic timescale τ_0 to reset the YORP strength for a kilometer-size member of the family. Therefore, $\boldsymbol{p} = (\boldsymbol{p}_1; \boldsymbol{p}_2) = (T, v_5, c_{\mathrm{YORP}}; \rho, \Gamma, \tau_0)$. The meaning of the first five parameters is straightforward. The last—τ_0—merits a brief explanation.

[7] We used The ATLAS Solar System Catalog (SSCAT) Version 2 available at https://astroportal.ifa.hawaii.edu/atlas/sscat/.

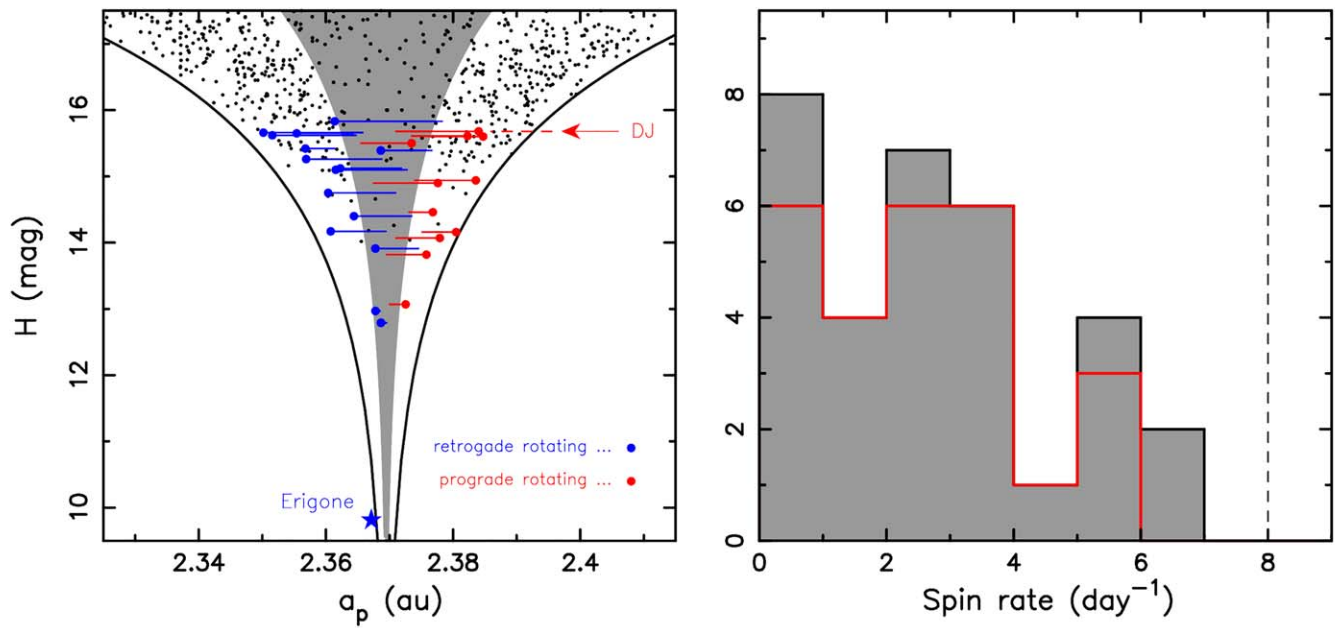

Figure 13. Left panel: segment of Erigone family projected onto the plane defined by the proper semimajor axis a_P (abscissa) and absolute magnitude H (ordinate; $H < 17.5$ mag zone shown). The black symbols are Erigone members observed by WISE constrained by two conditions: (i) $p_V \leqslant 0.125$, and (ii) with $|C| \leqslant |C_\star| = 1.7 \times 10^{-5}$ au (gray lines). The light-gray V-shaped zone is defined by $|C| \leqslant 5.2 \times 10^{-6}$ au, and it corresponds to the region in which the initial fragments from the family-forming event would land assuming an isotropic velocity field and ejection velocity $v_5 = 24$ m s^{-1} for $D = 5$ km asteroids (see Equation (5) in D. Vokrouhlický et al. 2006b). The color-highlighted asteroids with known spin state, sidereal rotation period, and pole orientations consist of DJ and objects listed in Table 1: the prograde- and retrograde-rotating cases are red and blue, respectively. The color intervals connect their current position to their past state $T = 155$ Myr ago using a simplified steady migration by the Yarkovsky effect fixing the present-day rotation state, bulk density $\rho = 1.5$ g cm^{-3}, and surface thermal inertia $\Gamma = 135$ SI (in the DJ case we assumed zero obliquity, but any value $\leqslant 20^\circ$ would lead to about the same conclusions). As expected, the prograde- and retrograde-rotating objects have $a_P > a_c$ and $a_P < a_c$, respectively, and their initial positions are in (or near) the initial velocity dispersal zone. Right panel: distribution of rotation rate values (abscissa; in rotations per day) for Erigone family members (except for (163) Erigone; gray histogram). The same for the subsample of asteroids with resolved rotation pole orientation in Table 1 is highlighted in red. The distribution is not compatible with that of the collisionally relaxed population, characterized by the Maxwellian function; rather, it bears similarity to the YORP-relaxed sample (see P. Pravec et al. 2008, for comparison). The vertical dashed line is the approximate rotation fission limit for low-density and low material cohesion asteroids.

W. F. Bottke et al. (2015b) developed what they called a "variable (or stochastic) YORP" approach, which was found to suit modeling the Eulalia family better than the traditional "static YORP" approach. In the latter case the characteristic strength of the YORP torques is kept constant over the asteroid's lifetime, while in the former case it is allowed to change on a characteristic timescale. This is because the magnitude of the YORP torques was found to be very sensitive to the small-scale surface topography (e.g., D. Vokrouhlický et al. 2015, for a review). Therefore, formation of new craters and the related surface shaking, which may cause landslides or boulder mobility, all may affect the YORP influence on small asteroids' rotation state evolution. W. F. Bottke et al. (2015b) thus considered a characteristic YORP-change timescale $\tau_{\rm YORP}$ over which they changed the YORP strength coefficient precomputed by D. Čapek & D. Vokrouhlický (2004). Since the essence of the effect may have to do with small (subcatastrophic) impacts, we additionally assume $\tau_{\rm YORP} = \tau_0 \sqrt{D}$, with τ_0 a free parameter and D the size in kilometers (the power exponent of the size dependence was motivated by analysis in P. Farinella et al. 1998). In our production simulations we consider τ_0 in the 0.5–100 Myr range (note that $\tau_0 \to \infty$ is the formal limit to the static approach of YORP modeling). An important implication of the variable YORP is a separation of the evolution of the obliquity and rotation rate timescales (see W. F. Bottke et al. 2015b; T. S. Statler 2015): while the obliquity evolves at the regular timescale of the static YORP variant, the rotation rate evolution is slowed down by effects of random walk. This helps the process of a small asteroid piling up to the semimajor axis extreme values in the family.

The model itself operates in the (a, H) plane, in which it initially (at the family formation) creates a synthetic population of 640 Erigone fragments centered about a_c and distributed in a. This model population has the same sizes D as the real Erigone members that contributed to construction of the $dN_{\rm sym}(C)$ distribution, each of them is ejected with velocity v_5 (5 km/D), and the initial velocity field is assumed isotropic. The fragments are also given initial rotation state parameters, namely (i) rotation period P from a Maxwellian distribution peaked at 6 hr, and (ii) obliquity γ corresponding to an isotropic distribution. Since the model fundamentally aims at describing the family dynamical evolution, the time t is let to advance in steps $dt = 0.1$ Myr. During this process, each fragment's (a; P, γ) are evolved: (i) semimajor axis a by the Yarkovsky effect, and (ii) (P, γ) by the YORP effect (details and complexities of this modeling are described in D. Vokrouhlický et al. 2006b; W. F. Bottke et al. 2015b). At regular time steps $dt' = 2$ Myr, the synthetic family population is mapped to the C-space, the corresponding distribution function $dM(C; \boldsymbol{p})$ is determined, and target function (3) is computed.

ORCID iDs

Simone Marchi https://orcid.org/0000-0003-2548-3291
David Vokrouhlický https://orcid.org/0000-0002-6034-5452
David Nesvorný https://orcid.org/0000-0002-4547-4301
William F. Bottke https://orcid.org/0000-0002-1804-7814

Josef Ďurech https://orcid.org/0000-0003-4914-3646
Harold F. Levison https://orcid.org/0000-0001-5847-8099

References

Ballouz, R. L., Walsh, K. J., Barnouin, O. S., et al. 2020, Bennu's Near-Earth Lifetime of 1.75 Million Years Inferred from Craters on Its Boulders, Natur, 587, 205

Benz, W., & Asphaug, E. 1994, Impact Simulations with Fracture. I. Method and Tests, Icar, 107, 98

Bolin, B. T., Delbo, M., Morbidelli, A., & Walsh, K. J. 2017, Yarkovsky V-shape Identification of Asteroid Families, Icar, 282, 290

Bolin, B. T., Morbidelli, A., & Walsh, K. J. 2018, Size-dependent Modification of Asteroid Family Yarkovsky V-shapes, A&A, 611, A82

Bottke, W. F., Brož, M., & O'Brien, D. P. 2015a, in Asteroids IV, ed. P. Michel, F. E. DeMeo, & W. F. Bottke (Tucson, AZ: Univ. Arizona Press), 701

Bottke, W. F., Durda, D. D., Nesvorný, D., et al. 2005b, The Fossilized Size Distribution of the Main Asteroid Belt, Icar, 175, 111

Bottke, W. F., Durda, D. D., Nesvorný, D., et al. 2005a, Linking the Collisional History of the Main Asteroid Belt to Its Dynamical Excitation and Depletion, Icar, 179, 63

Bottke, W. F., Vokrouhlický, D., Ballouz, R. L., et al. 2020, Interpreting the Cratering Histories of Bennu, Ryugu, and Other Spacecraft-explored Asteroids, AJ, 160, 14

Bottke, W. F., Vokrouhlický, D., & Nesvorný, D. 2007, An Asteroid Breakup 160 Myr Ago as the Probable Source of 1239 the K/T Impactor, Natur, 449, 48

Bottke, W. F., Vokrouhlický, D., Walsh, K. J., et al. 2015b, In Search of the Source of Asteroid (101955) Bennu: Applications of the Stochastic YORP Model, Icar, 247, 191

Brož, M., Vernazza, P., Marsset, M., et al. 2024a, Source Regions of Carbonaceous Meteorites and Near-Earth Objects, A&A, 689, A183

Brož, M., Vernazza, P., Marsset, M., et al. 2024b, Young Asteroid Families as the Primary Source of Meteorites, Natur, 634, 566

Čapek, D., & Vokrouhlický, D. 2004, The YORP Effect with Finite Thermal Conductivity, Icar, 172, 526

Carruba, V., Aljbaae, S., & Winter, O. C. 2016, On the Erigone Family and the z_2 Secular Resonance, MNRAS, 455, 2279

Carruba, V., Vokrouhlický, D., & Novaković, B. 2018, Asteroid Families Interacting with Secular Resonances, P&SS, 157, 72

Cellino, A., Bus, S. J., Doressoundiram, A., & Lazzaro, D. 2002, in Asteroids III, ed. W. F. Bottke, Jr. et al. (Tucson, AZ: Univ. Arizona Press), 633

Cellino, A., Dell'Oro, A., & Zappalà, V. 2004, Asteroid Families: Open Problems, P&SS, 52, 1075

Chapman, C. R., Merline, W. J., & Thomas, P. 1999, Cratering on Mathilde, Icar, 140, 28

Durda, D. D., Bottke, W. F., Enke, B. L., et al. 2004, The Formation of Asteroid Satellites in Large Impacts: Results from Numerical Simulations, Icar, 170, 243

Durda, D. D., Bottke, W. F., Nesvorný, D., et al. 2007, Size–Frequency Distributions of Fragments from SPH/N-body Simulations of Asteroid Impacts: Comparison with Observed Asteroid Families, Icar, 186, 498

Ďurech, J., & Hanuš, J. 2023, Reconstruction of Asteroid Spin States from Gaia DR3 Photometry, A&A, 675, A24

Ďurech, J., Sidorin, V., & Kaasalainen, M. 2010, DAMIT: A Database of Asteroid Models, A&A, 513, A46

Ďurech, J., Tonry, J., Erasmus, N., et al. 2020, Asteroid Models Reconstructed from ATLAS Photometry, A&A, 643, A59

Ďurech, J., Vokrouhlický, D., Pravec, P., et al. 2022, Rotation Acceleration of Asteroids (10115) 1992 SK, (1685) Toro, and (1620) Geographos due to the YORP Effect, A&A, 657, A5

Farinella, P., & Davis, D. R. 1992, Collision Rates and Impact Velocities in the Main Asteroid Belt, Icar, 97, 111

Farinella, P., Vokrouhlický, D., & Hartmann, W. K. 1998, Meteorite Delivery via Yarkovsky Orbital Drift, Icar, 132, 378

Farnocchia, D., Vokrouhlický, D., Čapek, D., Chesley, S. R., & DellaGiustina, D. N. 2024, in LPI Contributions 3006, Apophis T-5 Workshop, 2046

Ferrais, M., Jehin, E., Manfroid, J., et al. 2021, AAS/DPS Meeting, 53, 306.19

Gallardo, T., Venturini, J., Roig, F., & Gil-Hutton, R. 2011, Origin and Sustainability of the Population of Asteroids Captured in the Exterior Resonance 1:2 with Mars, Icar, 214, 632

Hanuš, J., Vokrouhlický, D., Nesvorný, D., et al. 2023, Shape Models and Spin States of Jupiter Trojans. Testing the Streaming Instability Formation Scenario, A&A, 679, A56

Harvison, B., De Prá, M., Pinilla-Alonso, N., et al. 2024, PRIMASS Near-infrared Study of the Erigone Collisional Family, Icar, 412, 115973

Hendler, N. P., & Malhotra, R. 2020, Observational Completion Limit of Minor Planets from the Asteroid Belt to Jupiter Trojans, PSJ, 1, 75

Hirayama, K. 1918, Groups of Asteroids Probably of Common Origin, AJ, 31, 185

Holsapple, K. A., & Housen, K. R. 2007a, A Crater and Its Ejecta: An Interpretation of Deep Impact, Icar, 187, 345

Holsapple, K. A., & Housen, K. R. 2007b, A Crater and Its Ejecta: An Interpretation of Deep Impact, Icar, 191, 586

Jutzi, M., Holsapple, K., Wünneman, K., & Michel, P. 2015, in Asteroids IV, ed. P. Michel, F. E. DeMeo, & W. F. Bottke (Tucson, AZ: Univ. Arizona Press), 679

Kaasalainen, M., Torppa, J., & Muinonen, K. 2001, Optimization Methods for Asteroid Lightcurve Inversion. II. The Complete Inverse Problem, Icar, 153, 37

Knežević, Z., & Milani, A. 2000, Synthetic Proper Elements for Outer Main Belt Asteroids, CeMDA, 78, 17

Knežević, Z., & Milani, A. 2003, Proper Element Catalogs and Asteroid Families, A&A, 403, 1165

Lauretta, D. S., Dellagiustina, D. N., Bennett, C. A., et al. 2019, The Unexpected Surface of Asteroid (101955) Bennu, Natur, 568, 55

Leinhardt, Z. M., & Richardson, D. C. 2002, N-body Simulations of Planetesimal Evolution: Effect of Varying Impactor Mass Ratio, Icar, 159, 306

Leinhardt, Z. M., Richardson, D. C., & Quinn, T. 2000, Direct N-body Simulations of Rubble Pile Collisions, Icar, 146, 133

Levison, H. F., Marchi, S., Noll, K. S., et al. 2024, A Contact Binary Satellite of the Asteroid (152830) Dinkinesh, Natur, 629, 1015

Levison, H. F., Olkin, C. B., Noll, K. S., et al. 2021, Lucy Mission to the Trojan Asteroids: Science Goals, PSJ, 2, 171

Mainzer, A., Grav, T., Bauer, J., et al. 2011, NEOWISE Observations of Near-Earth Objects: Preliminary Results, ApJ, 743, 156

Marchi, S., Chapman, C. R., Barnouin, O. S., Richardson, J. E., & Vincent, J. B. 2015, in Asteroids IV, ed. P. Michel, F. E. DeMeo, & W. F. Bottke (Tucson, AZ: Univ. Arizona Press), 725

Marchi, S., Nesvorný, D., Vokrouhlický, D., Bottke, W. F., & Levison, H. 2023, A Crater Chronology for the Jupiter's Trojan Asteroids, AJ, 166, 221

Marchi, S., Paolicchi, P., Lazzarin, M., & Magrin, S. 2006, A General Spectral Slope-exposure Relation for S-type Main Belt and Near-Earth Asteroids, AJ, 131, 1138

Marzari, F., Farinella, P., & Davis, D. R. 1999, Origin, Aging, and Death of Asteroid Families, Icar, 142, 63

Masiero, J. R., DeMeo, F. E., Kasuga, T., & Parker, A. H. 2015, in Asteroids IV, ed. P. Michel, F. E. DeMeo, & W. F. Bottke (Tucson, AZ: Univ. Arizona Press), 323

Masiero, J. R., Mainzer, A. K., Bauer, J. M., et al. 2013, Asteroid Family Identification Using the Hierarchical Clustering Method and WISE/NEOWISE Physical Properties, ApJ, 770, 7

Masiero, J. R., Mainzer, A. K., Grav, T., et al. 2011, Main Belt Asteroids with WISE/NEOWISE. I. Preliminary Albedos and Diameters, ApJ, 741, 68

Milani, A., Cellino, A., Knežević, Z., et al. 2014, Asteroid Families Classification: Exploiting Very Large Datasets, Icar, 239, 46

Milani, A., & Knežević, Z. 1992, Asteroid Proper Elements and Secular Resonances, Icar, 98, 211

Milani, A., & Knežević, Z. 1994, Asteroid Proper Elements and the Dynamical Structure of the Asteroid Main Belt, Icar, 107, 219

Milani, A., Knežević, Z., Spoto, F., & Paolicchi, P. 2019, Asteroid Cratering Families: Recognition and Collisional Interpretation, A&A, 622, A47

Milani, A., & Nobili, A. M. 1992, An Example of Stable Chaos in the Solar System, Natur, 357, 569

Morate, D., de León, J., De Prá, M., et al. 2016, Compositional Study of Asteroids in the Erigone Collisional Family Using Visible Spectroscopy at the 10.4 m GTC, A&A, 586, A129

Morbidelli, A., & Nesvorný, D. 1999, Numerous Weak Resonances Drive Asteroids toward Terrestrial Planets Orbits, Icar, 139, 295

Morbidelli, A., Walsh, K. J., O'Brien, D. P., Minton, D. A., & Bottke, W. F. 2015, The Dynamical Evolution of the Asteroid Belt, in Asteroids IV, ed. P. Michel, F. E. DeMeo, & W. F. Bottke (Tucson, AZ: Univ. Arizona Press), 493

Naidu, S. P., Chesley, S. R., & Farnocchia, D. 2017, AAS/DPS Meeting, 49, 112.04

Nesvorný, D., Bottke, W. F., Levison, H. F., & Dones, L. 2003, Recent Origin of the Solar System Dust Bands, ApJ, 591, 486

Nesvorný, D., Brož, M., & Carruba, V. 2015, in Asteroids IV, ed. P. Michel, F. E. DeMeo, & W. F. Bottke (Tucson, AZ: Univ. Arizona Press), 297

Nesvorný, D., & Morbidelli, A. 1998, Three-body Mean Motion Resonances and the Chaotic Structure of the Asteroid Belt, AJ, 116, 3029
Nesvorný, D., Roig, F., Vokrouhlický, D., & Brož, M. 2024a, Catalog of Proper Orbits for 1.25 Million Main-belt Asteroids and Discovery of 136 New Collisional Families, ApJS, 274, 25
Nesvorný, D., Vokrouhlický, D., Shelly, F., et al. 2024b, NEOMOD 2: An Updated Model of Near-Earth Objects from a Decade of Catalina Sky Survey Observations, Icar, 411, 115922
Novaković, B., Vokrouhlický, D., Spoto, F., & Nesvorný, D. 2022, Asteroid Families: Properties, Recent Advances, and Future Opportunities, CeMDA, 134, 34
Okada, T., Fukuhara, T., Tanaka, S., et al. 2020, Highly Porous Nature of a Primitive Asteroid Revealed by Thermal Imaging, Natur, 579, 518
Paolicchi, P., & Knežević, Z. 2016, Footprints of the YORP Effect in Asteroid Families, Icar, 274, 314
Paolicchi, P., Spoto, F., Knežević, Z., & Milani, A. 2019, Ages of Asteroid Families Estimated Using the YORP-eye Method, MNRAS, 484, 1815
Parker, A., Ivezić, Ž., Jurić, M., et al. 2008, The Size Distributions of Asteroid Families in the SDSS Moving Object Catalog 4, Icar, 198, 138
Perry, M. E., Barnouin, O. S., Daly, R. T., et al. 2022, Low Surface Strength of the Asteroid Bennu Inferred from Impact Ejecta Deposit, NatGe, 15, 447
Polishook, D., Moskovitz, N., Binzel, R. P., et al. 2014, Observations of "Fresh" and Weathered Surfaces on Asteroid Pairs and Their Implications on the Rotational-fission Mechanism, Icar, 233, 9
Pravec, P., Fatka, P., Vokrouhlický, D., et al. 2019, Asteroid Pairs: A Complex Picture, Icar, 333, 429
Pravec, P., Harris, A. W., Vokrouhlický, D., et al. 2008, Spin Rate Distribution of Small Asteroids, Icar, 197, 497
Pravec, P., Scheirich, P., Ďurech, J., et al. 2014, The Tumbling Spin State of (99942) Apophis, Icar, 233, 48
Press, W. H., Teukolsky, S. A., Vetterling, W. T., & Flannery, B. P. 2007, Numerical Recipes: The Art of Scientific Computing (Cambridge: Cambridge Univ. Press)
Richardson, D. C., Quinn, T., Stadel, J., & Lake, G. 2000, Direct Large-scale N-body Simulations of Planetesimal Dynamics, Icar, 143, 45
Roberts, J. H., Barnouin, O. S., Daly, M. G., et al. 2021, Rotational States and Shapes of Ryugu and Bennu: Implications for Interior Structure and Strength, P&SS, 204, 105268
Rozitis, B., Ryan, A. J., Emery, J. P., et al. 2020, Bennu's Weak Boulders and Thermally Anomalous Equator, SciA, 6, eabc3699
Scheeres, D. J., French, A. S., Tricarico, P., et al. 2020, Heterogeneous Mass Distribution of the Rubble-pile Asteroid (101955) Bennu, SciA, 6, eabc3350
Shimaki, Y., Senshu, H., Sakatani, N., et al. 2020, Thermophysical Properties of the Surface of Asteroid 162173 Ryugu: Infrared Observations and Thermal Inertia Mapping, Icar, 348, 113835
Spoto, F., Milani, A., & Knežević, Z. 2015, Asteroid Family Ages, Icar, 257, 275
Stadel, J. G. 2001, PhD thesis, Univ. of Washington, Seattle
Statler, T. S. 2015, Obliquities of "Top-shaped" Asteroids May Not Imply Reshaping by YORP Spin-up, Icar, 248, 313
Takir, D., Emery, J. P., Bottke, W. F., & Arredondo, A. 2024, Origin of Asteroid (101955) Bennu and its Connection to the New Polana Family, NatSR, 14, 15965
Tatsumi, E., Sugimoto, C., Riu, L., et al. 2021, Collisional History of Ryugu's Parent Body from Bright Surface Boulders, NatAs, 5, 39
Vokrouhlický, D., Bottke, W. F., Chesley, S. R., Scheeres, D. J., & Statler, T. S. 2015, in Asteroids IV, ed. P. Michel, F. E. DeMeo, & W. F. Bottke (Tucson, AZ: Univ. Arizona Press), 509
Vokrouhlický, D., Breiter, S., Nesvorný, D., & Bottke, W. F. 2007, Generalized YORP Evolution: Onset of Tumbling and New Asymptotic States, Icar, 191, 636
Vokrouhlický, D., & Brož, M. 2002, Interaction of the Yarkovsky-drifting Orbits with Weak Resonances: Numerical Evidence and Challenges, in Modern Celestial Mechanics: from Theory to Applications, ed. A. Celletti, S. Ferraz-Mello, & J. Henrard (Dordrecht: Kluwer), 467
Vokrouhlický, D., Brož, M., Bottke, W. F., Nesvorný, D., & Morbidelli, A. 2006a, The Peculiar Case of the Agnia Asteroid Family, Icar, 183, 349
Vokrouhlický, D., Brož, M., Morbidelli, A., et al. 2006b, Yarkovsky Footprints in the Eos Family, Icar, 182, 92
Vokrouhlický, D., Nesvorný, D., Brož, M., & Bottke, W. F. 2024, Debiased Population of Very Young Asteroid Families, A&A, 681, A23
Walsh, K. J., Delbó, M., Bottke, W. F., Vokrouhlický, D., & Lauretta, D. S. 2013, Introducing the Eulalia and New Polana Asteroid Families: Re-assessing Primitive Asteroid Families in the Inner Main Belt, Icar, 225, 283
Warner, B. D., Harris, A. W., & Pravec, P. 2009, The Asteroid Lightcurve Database, Icar, 202, 134
Watanabe, S., Hirabayashi, M., Hirata, N., et al. 2019, Hayabusa2 Arrives at the Carbonaceous Asteroid 162173 Ryugu—A Spinning Top-shaped Rubble Pile, Sci, 364, 268
Weaver, H. A., Wilson, J. P., Conard, S. J., et al. 2023, The Lucy Long Range Reconnaissance Imager (L'LORRI), SSRv, 219, 82
Williams, J. G. 1979, in Asteroids, ed. T. Gehrels & M. S. Matthews (Tucson, AZ: Univ. Arizona Press), 1040
Williams, J. G. 1992, Asteroid Families—An Initial Search, Icar, 96, 251
Williams, J. G., & Hierath, J. E. 1987, Palomar-Leiden Minor Planets: Proper Elements, Frequency Distributions, Belt Boundaries, and Family Memberships, Icar, 72, 276
Zappalà, V., Cellino, A., Farinella, P., & Knežević, Z. 1990, Asteroid Families. I. Identification by Hierarchical Clustering and Reliability Assessment, AJ, 100, 2030